Field Demonstration of an Innovative Box Beam Connection

Final Report
February 2023

IOWA STATE UNIVERSITY

Institute for Transportation

About the Bridge Engineering Center

The mission of the Bridge Engineering Center (BEC) is to conduct research on bridge technologies to help bridge designers/owners design, build, and maintain long-lasting bridges.

About the Institute for Transportation

The mission of the Institute for Transportation (InTrans) at Iowa State University is to save lives and improve economic vitality through discovery, research innovation, outreach, and the implementation of bold ideas.

Iowa State University Nondiscrimination Statement

Iowa State University does not discriminate on the basis of race, color, age, ethnicity, religion, national origin, pregnancy, sexual orientation, gender identity, genetic information, sex, marital status, disability, or status as a US veteran. Inquiries regarding nondiscrimination policies may be directed to the Office of Equal Opportunity, 3410 Beardshear Hall, 515 Morrill Road, Ames, Iowa 50011, telephone: 515-294-7612, hotline: 515-294-1222, email: eooffice@iastate.edu.

Disclaimer Notice

The contents of this report reflect the views of the authors, who are responsible for the facts and the accuracy of the information presented herein. The opinions, findings and conclusions expressed in this publication are those of the authors and not necessarily those of the sponsors.

The sponsors assume no liability for the contents or use of the information contained in this document. This report does not constitute a standard, specification, or regulation.

The sponsors do not endorse products or manufacturers. Trademarks or manufacturers' names appear in this report only because they are considered essential to the objective of the document.

Iowa DOT Statements

Federal and state laws prohibit employment and/or public accommodation discrimination on the basis of age, color, creed, disability, gender identity, national origin, pregnancy, race, religion, sex, sexual orientation or veteran's status. If you believe you have been discriminated against, please contact the Iowa Civil Rights Commission at 800-457-4416 or Iowa Department of Transportation's affirmative action officer. If you need accommodations because of a disability to access the Iowa Department of Transportation's services, contact the agency's affirmative action officer at 800-262-0003.

The preparation of this report was financed in part through funds provided by the Iowa Department of Transportation through its "Second Revised Agreement for the Management of Research Conducted by Iowa State University for the Iowa Department of Transportation" and its amendments.

The opinions, findings, and conclusions expressed in this publication are those of the authors and not necessarily those of the Iowa Department of Transportation.

Technical Report Documentation Page

1. Report No. IHRB Project TR-743	2. Government Accession No.	3. Recipient's Catalog No.	
4. Title and Subtitle Field Demonstration of an Innovative Box Beam Connection		**5. Report Date** February 2023	
		6. Performing Organization Code	
7. Author(s) Zhengyu Liu (orcid.org/0000-0002-7407-0912), Justin Dahlberg (orcid.org/0000-0002-6184-4122), and Brent M. Phares (orcid.org/0000-0001-5894-4774)		**8. Performing Organization Report No.** InTrans Project 18-647	
9. Performing Organization Name and Address Bridge Engineering Center Iowa State University 2711 South Loop Drive, Suite 4700 Ames, IA 50010-8664		**10. Work Unit No. (TRAIS)**	
		11. Contract or Grant No.	
12. Sponsoring Organization Name and Address Iowa Highway Research Board Iowa Department of Transportation 800 Lincoln Way Ames, IA 50010		**13. Type of Report and Period Covered** Final Report	
		14. Sponsoring Agency Code IHRB Project TR-743	

15. Supplementary Notes

Visit https://bec.intrans.iastate.edu/ for color pdfs of this and other research reports.

16. Abstract

The objective of this project was to demonstrate the field implementation of an innovative longitudinal joint design developed during a previous phase of research. To achieve this objective, a yet-to-be-constructed box girder bridge in Washington County, Iowa, was selected to demonstrate the construction and performance of the joint.

In order to evaluate the joint's performance, a seven-day period of field monitoring was conducted shortly after construction was completed. In addition, long-term evaluation of the joint was performed through the completion of live load field tests and deck concrete crack inspections. The live load tests were performed every 12 months, and crack inspections of the bridge deck were performed every six months. During the field tests and monitoring, temperature, strain, and displacement data were collected at critical locations and analyzed to evaluate joint performance with respect to cracking resistance and load distribution.

The results indicate that the innovative joint is sufficient to resist early-age longitudinal joint cracking. Joint cracks that were seen on another box girder bridge with traditional narrow joints were not observed in this case. The innovative joint performed well with respect to load distribution. The whole bridge superstructure behaved as an integrated structure regardless of the transverse location of a passing truck. In addition, the box girder bridge was constructed using integral abutments, which added transverse restraint and positively affected the strain distribution at the joint ends.

17. Key Words adjacent box girder bridge—box beam connection—early age concrete performance—field testing—Type K cement	**18. Distribution Statement** No restrictions.		
19. Security Classification (of this report) Unclassified.	**20. Security Classification (of this page)** Unclassified.	**21. No. of Pages** 56	**22. Price** NA

Form DOT F 1700.7 (8-72)   Reproduction of completed page authorized

FIELD DEMONSTRATION OF AN INNOVATIVE BOX BEAM CONNECTION

Final Report
February 2023

Principal Investigator
Brent M. Phares, Research Associate Professor
Civil, Construction, and Environmental Engineering, Iowa State University

Primary Researchers
Zhengyu Liu, Senior Research Scientist
Bridge Engineer Center, Iowa State University

Justin Dahlberg, Director
Bridge Engineer Center, Iowa State University

Authors
Zhengyu Liu, Justin Dahlberg, and Brent M. Phares

TABLE OF CONTENTS

LIST OF FIGURES

LIST OF TABLES

ACKNOWLEDGMENTS

EXECUTIVE SUMMARY

The objective of this project was to demonstrate the field implementation of an innovative longitudinal joint design developed during a previous phase of research. To achieve this objective, a yet-to-be-constructed box girder bridge in Washington County, Iowa, was selected to demonstrate the construction and performance of the joint.

In order to evaluate the joint's performance, a seven-day period of field monitoring was conducted shortly after construction was completed. In addition, long-term evaluation of the joint was performed through the completion of live load field tests and deck concrete crack inspections. The live load tests were performed every 12 months, and crack inspections of the bridge deck were performed every six months. During the field tests and monitoring, temperature, strain, and displacement data were collected at critical locations and analyzed to evaluate joint performance with respect to cracking resistance and load distribution.

The results indicate that the innovative joint is sufficient to resist early-age longitudinal joint cracking. Joint cracks that were seen on another box girder bridge with traditional narrow joints were not observed in this case. The innovative joint performed well with respect to load distribution. The whole bridge superstructure behaved as an integrated structure regardless of the transverse location of a passing truck. In addition, the box girder bridge was constructed using integral abutments, which added transverse restraint and positively affected the strain distribution at the joint ends.

CHAPTER 1. INTRODUCTION

1.1 Background

Adjacent concrete box beam bridges constitute more than 15% of the bridges built or replaced each year. This type of bridge is generally constructed by placing box beams next to one another, grouting adjoining shear keys, applying a transverse post-tensioning force, and then, perhaps, placing a thin wearing surface or a thick (6 in.) structural deck. Historically, these and other similar adjacent precast elements have suffered from differential displacements, which cause cracking in adjoining joint material (or, in some cases, in the cast-in-place topping material).

A significant amount of information related to adjacent box beams was reviewed in Phase I of this research study (Phares et al. 2017, Liu 2018), and the preliminary findings are presented and summarized here. Cracking in the joint between adjacent box beams appears to principally be a service-related problem, and even with a cracked joint, a bridge can continue to distribute loads effectively throughout the primary load-carrying members (Huckelbridge et al. 1995). With regards to cracking, it appears that cracking tends to be most prominent at the interface between the joint material and the box beam due to apparent low bond strength (Attanayake and Aktan 2008, Sharp 2007). The use of a shear key may induce stress concentrations in the joint (Dong and Ahlborn 2007). Consistent throughout the literature is the conclusion that the joints that use full-depth keyways have the best performance (El-Remaily et al. 1996, Lall et al. 1998, Hanna et al. 2011, Hansen et al. 2012). The use of transverse post-tensioning can induce transverse tensile stress and cracks since the uniform distribution of the post-tension force at the keyway cannot always be guaranteed (Ulku et al. 2010, Grace et al. 2012). Cracking does not seem to be initiated by the application of live loads and is suspected to be caused by low bond strength between the joint material and box girder, large shrinkage of the joint material, stress concentrations near the shear key, and temperature changes. There are, however, differing opinions on the relative contribution to cracking from shrinkage and temperature. Nevertheless, once cracking is initiated, cracks can continue to grow with subsequent live load applications (Miller et al. 1999, Sharpe 2007, Attanayake and Aktan 2008, Grace et al. 2012).

Until recently, the addition of a structural deck has been the only nearly guaranteed way to eliminate problematic cracking. However, the structural deck adds high cost, construction time, and bridge dead load. More recently, a new joint detail was developed and tested by the Federal Highway Administration (FHWA) (Yuan et al. 2018). The only potential drawback to the developed system is that its performance requires the use of so-called ultra-high performance concrete (UHPC). While UHPC provides many qualities that are far superior to those of conventional (and high-performance) concretes, the cost of the material is up to 10 times greater. Additionally, UHPC requires special mixing equipment and is best placed by experienced field staff (Phares et al. 2017, Liu and Phares 2022, Liu et al. 2022).

Liu and Phares (2020) conducted multiple levels of material tests and developed a finite element (FE) modeling approach capable of simulating early-age joint behavior to select the most suitable crack-resistant material associated with various joint geometries. The results indicated that a 6½ in. wide joint filled with shrinkage-compensating concrete performed better than all the

other choices. Liu and Phares (2019) designed an innovative 6½ in. wide joint without a shear key that incorporated concepts such as shrinkage-compensating concrete achieved by using Type K cement, the use of form retarder to create a rough surface on the sides of the box girder to increase shear and bond capacity, and reinforcing steel bars that cross the interface between the joint and box girder. The innovation is especially apparent when the joint is compared to the traditional longitudinal joint used in the United States, which has a narrow width of ¾ in. to 1½ in. and shrinkage material with post-tensioning but no reinforcing steel in the joint. The innovative design was evaluated in a series of small-scale tests and analytical models with different joint reinforcement ratios. The early-age joint behavior was monitored, and an ultimate load test was performed. Both experimental and FE results indicated that the developed joint with No. 4 transverse bars placed at a 9.0 in. spacing provides satisfactory performance in resisting early-age joint cracks.

Ending in 2017, the Iowa State University Bridge Engineering Center performed a series of laboratory tests on the innovative joint that replicated the testing completed by the FHWA (Yuan et al. 2018), including temperature loading, vertical cyclic loading, and horizontal loading. Specifically, to simulate early-age environmental and curing conditions, temperature loading was applied immediately after joint material placement such that early-age concrete expansion, the heat of hydration, and concrete hardening were all occurring simultaneously (conditions in which cracking has commonly been observed to develop). During temperature testing, a vertical temperature gradient of 40°F was simulated and applied to the specimen. This testing continued for seven days, and no cracking was observed (Liu et al. 2020, Shi et al. 2019). Cyclic loading was applied with the connected beams in a simply supported condition. After the application of 5,000,000 cycles of loads up to 42 kips, no cracking was observed. Then, one of the beams was restrained (as the FHWA had done), and cyclic loading was continued. With no cracking observed, the beam was finally loaded with a direct horizontal load, which ultimately crushed the beam's concrete without cracking the joint material (Liu et al. 2020, Shi et al. 2020).

1.2 Objective and Approach

The objective of this project was to design, construct, and evaluate the performance of a yet-to-be-constructed box girder bridge in Washington County, Iowa. The specific objectives associated with this work were as follows:

- Assist the design engineer in finalizing the innovative longitudinal joint design
- Document important construction procedures and operations
- Evaluate the on-site joint performance
- Disseminate information to Iowa counties and others interested in the results

1.3 Research Plan and Deliverables

In order to achieve the objectives listed above, a multi-task research plan was completed with a primary focus on bridge design completion, field monitoring, and performance evaluation. This report documents the project tasks, results, and conclusions.

1.4 Report Outline

This report includes the following chapters:

Chapter 1: Introduction
Chapter 2: Bridge Design and Longitudinal Joint Design
Chapter 3: Early-Age Performance Monitoring
Chapter 4: Long-Term Performance Evaluation (Live Load Testing)
Chapter 5: Summary and Conclusions

The results from Task 2 of the research plan are documented in Chapter 2, and the results from Task 3 are documented in Chapter 3 and Chapter 4 for early-age and long-term performance, respectively.

CHAPTER 2. BRIDGE DESIGN AND LONGITUDINAL JOINT DETAILS

Procedures and operations observed during the construction of the Washington County bridge are documented in this chapter. This documentation serves two primary purposes: (1) to show that the bridge was constructed with relative ease and (2) to serve as a "how-to" for counties interested in constructing future bridges using their own resident construction crews.

2.1 General Bridge Information

During completion of the Phase I work, HDR, Inc. was developing box beam standards for the Iowa DOT that utilize the previously mentioned FHWA connection detail. For simplicity and ease of use, the detail developed by Iowa State University was established for direct integration into those standards, with only minor geometric modifications needed. To the best of the research team's knowledge, the work described here is the first to utilize those standards. The standards were used with only minor changes to the joint geometry when the bridge in Washington County, Iowa, was designed.

The bridge is single-span, 32 ft wide, and 70 ft long. The bridge superstructure consists of eight 4 ft wide box beams. Figure 1 shows a cross-section view of the bridge superstructure with labels for each box girder and joint. The bridge does not have a skew.
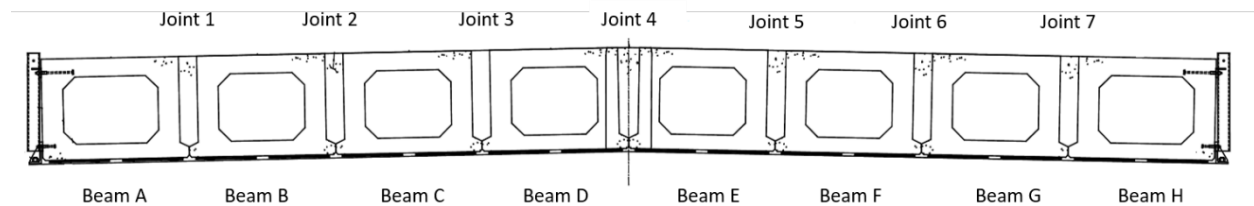

Figure 1. Bridge cross-section view

2.2 Longitudinal Joint Design

The innovative joint in the Washinton County bridge is consistent with the one designed by Liu (2018). Figure 2 shows a three-dimensional (3D) view of the joint details. This joint was designed based on the well-known wide, full-depth joint without a deck. The shrinkage-compensating concrete was developed based on the standard Iowa DOT C4 concrete mix design, with 15% of the traditional portland cement replaced by Type K shrinkage-compensating cement to minimize or eliminate the shrinkage typically associated with normal concrete. Note that the magnitude of shrinkage or expansion can be controlled by adjusting the amount of the portland cement replaced by Type K cement.
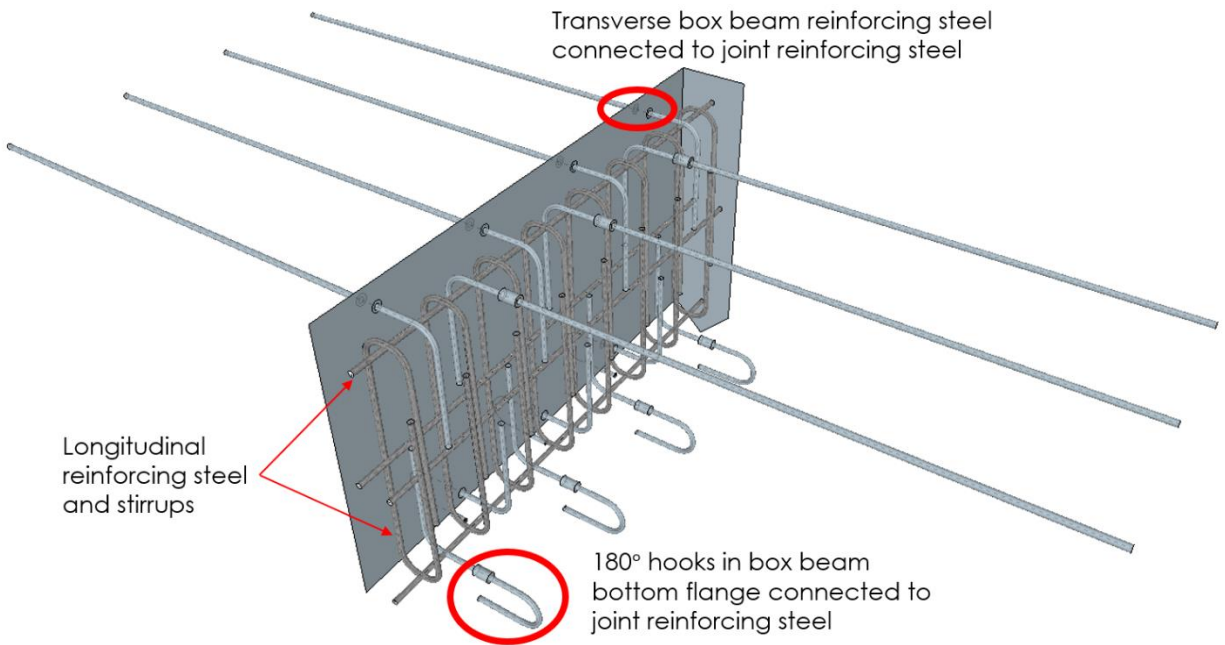
Phares et al. 2017

Figure 2. Innovative longitudinal joint

To enhance the shear transfer capability, the flat interface was roughened using a form retarder followed by pressure washing. The form retarder inhibits the hydration of the cement between the aggregate near the surface of the fresh concrete. The unhydrated paste can then be easily removed when washed. The aggregate was left protruding about 1.9 to 2.5 cm (0.75 to 1 in.). To provide transverse restraint and generate a large compression zone associated with the expanding material in the early-age joint, transverse reinforcing steel across the interface was included.

Figure 3 shows the cross-section design and reinforcement arrangement in the box girders. A long straight bar was placed at the top of the box girders, and a 180° hook bar was placed at the bottom. Both the straight bars and 180° hook bars were connected to 90° hook bars in the joints by commercially available couplers before setting the beams on the supports. The coupler connection ensures that the strength of the connection is at least as high as that of the bar alone. Longitudinal reinforcing steel and stirrups were placed in the joints to create internally reinforced beams within the joints. During bridge construction in the field, the straight bar and 180° hook bar can be pre-embedded into the precast box beams. The 90° hook bars can easily be installed either in the factory or in the field prior to placement of the prestressed box beams on the piers.
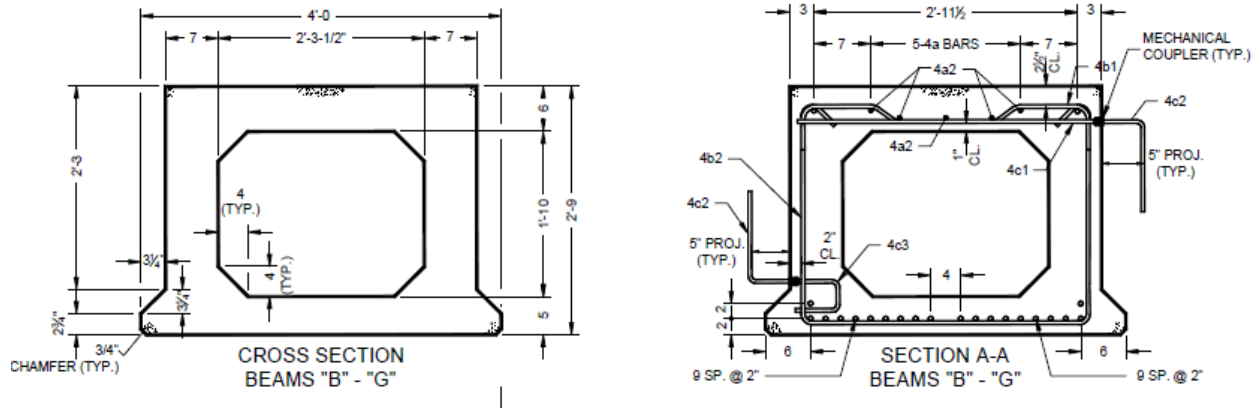
Figure 3. Cross-section design and reinforcement arrangement in the box girders

Unlike in the design by Liu (2018), where the 90° hook bars are spaced at 8.0 in. near the ends of the beams and at 1 ft at the mid-span, in the Washington County bridge the joints' 90° hook bars were placed with a consistent spacing of 9 in. to avoid any confusion during bridge design and construction.

2.3 Bridge Construction

The research team observed the fabrication of the box girders and the placement of the joint concrete. Although this special design was previously constructed in a laboratory environment, this was the first time that it was fabricated in a concrete plant and deployed on-site at an in-service bridge. Therefore, the construction activities related to the implementation of the special joint are documented and presented in this section.

2.3.1 Prefabrication of the Box Girder

The prestressed box girders were cast in a precast concrete plant. Two girders were cast at four different times due to the capacity and labor limitations of the manufacturer. Figure 4 shows a timeline of milestone events during beam manufacturing and bridge construction. The box girders were cast between August 20, 2020, and September 2, 2020, and were delivered to the field on October 1, 2020. The first girders were more than 28 days old when they were delivered.
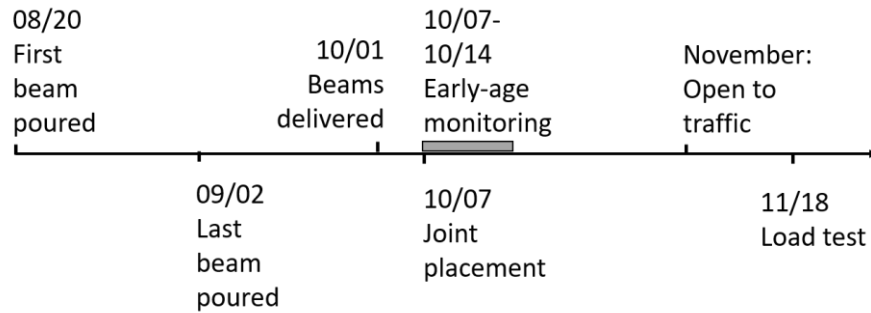
Figure 4. Timeline for bridge construction, monitoring, and load testing

Figure 5 shows photographs of the girder fabrication. For each girder, the box girder concrete was placed into a steel form, as shown in Figure 5a. Boards were attached to the side of the steel form to form the shape of the wide joint. A large polyethylene form was used in the middle to create the void of the box girder. The formwork was completed by using cross-steel frames to resist the fluid concrete pressure, as shown in Figure 5b. Figure 5c shows the concrete placement. The process was completed when the surface was hand-troweled, as shown in Figure 5d.

(a) Box girder reinforcement placement

(b) Internal box

(c) Box girder concrete placement

(d) Surface completion

Figure 5. Prefabrication of box girder

2.3.2 Field Construction of Longitudinal Joints

The beams were delivered to the field on October 1, 2020 (Figure 6a). Before the beams were placed in position, the 90° hook bars were screwed into the dowel bars embedded into the precast

box girders. After the beams were placed in position, the joint reinforcement, including the stirrups and the longitudinal straight rebar, was installed, as shown in Figure 6b.

In order to hold the fresh concrete in the joints, timber boards were attached to the ends of the box girders. These boards were anchored into the ends of the girders, as shown in Figure 6c. Figure 6d shows an overview of the bridge superstructure before the placement of the joint material and abutment concrete.

(a) Box girders placed
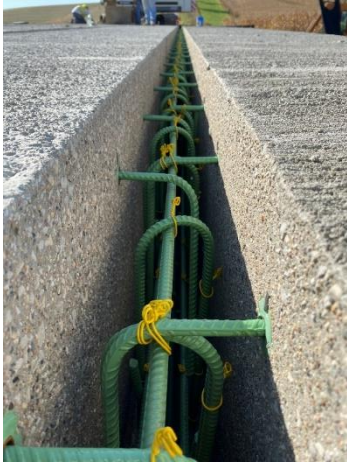
(b) Joint reinforcement

(c) Plywood forms at the ends of the joints

(d) Bridge before placement of joint concrete

Figure 6. Longitudinal joints before placement of joint material

The joint material placement work was completed on October 7, 2020, starting at 8:30 a.m. Figure 7 shows the time of placement for each joint. In total, the joint completion took about 3 hours and 40 minutes, ending at 12:10 p.m. Nearly 30 yd^3 of concrete were required to complete the joints.
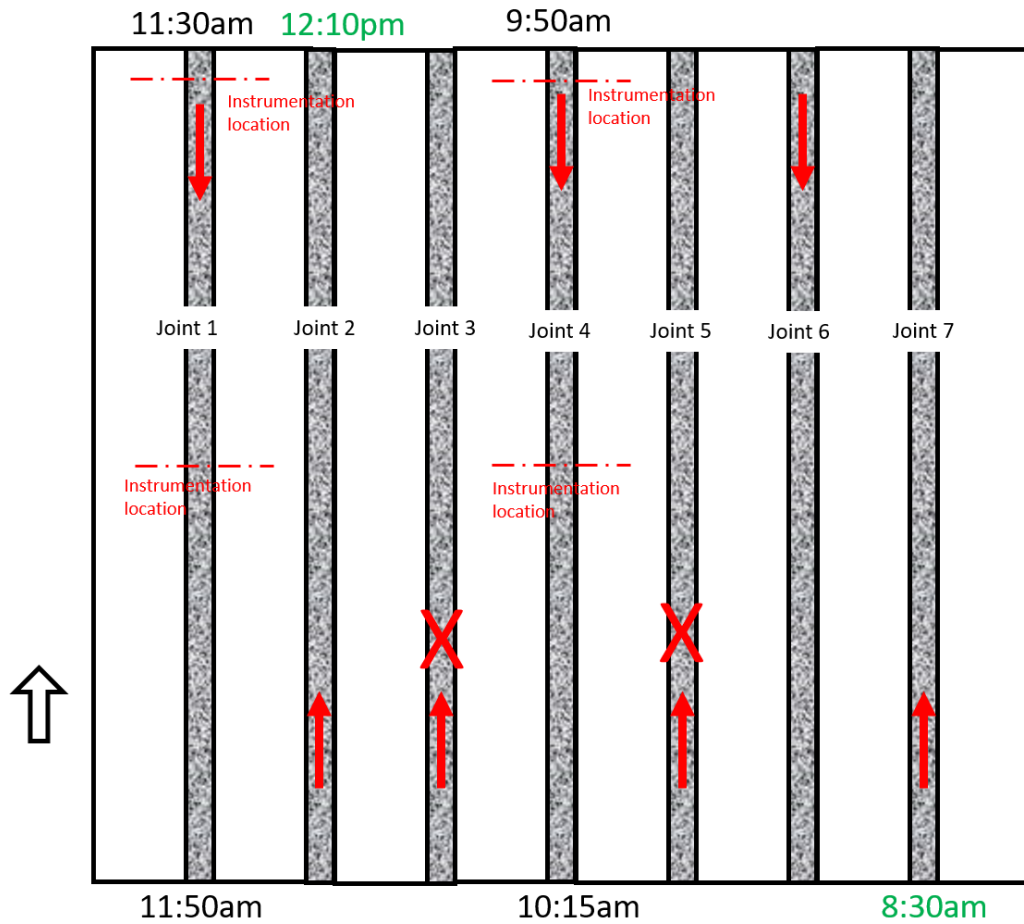
Figure 7. Joint placement timeline

As shown in Figure 7, joint placement started from the south side of Joint 7 on the east side of the bridge and continued to the joints on the west side. In the end, Joint 1 was placed before Joint 2, and Joint 2 was the last joint to be poured.

Consistent with the work conducted by Liu (2018), the shrinkage-compensating concrete was developed based on the standard Iowa DOT C4 concrete mix design, with 15% of the traditional portland cement replaced by Type K shrinkage-compensating cement (as shown in Table 1) to minimize or eliminate the shrinkage typically associated with normal concrete. Table 1 shows the mix design for the Iowa DOT C4 concrete and the shrinkage-compensating concrete. Note that the amount of shrinkage or expansion can be controlled by adjusting the amount of the portland cement replaced by Type K cement.

Table 1. Joint concrete mix design

Component (kg/m³ [lb/yd³])	Iowa DOT C4	Shrinkage-compensating concrete
Portland cement	235 (474)	200 (403)
Fly ash	59 (119)	59 (119)
Water	126 (255)	126 (255)
Fine aggregate	744 (1500)	744 (1500)
Coarse aggregate	753 (1517)	753 (1517)
Type K cement	—	35 (71)

Figure 8 shows the labor workforce placing the joint concrete.

(a) Placement of joint concrete

(b) Concrete transfer from truck to bucket

(c) Lifting equipment to move bucket

(d) Work crew during concrete placement

Figure 8. Joint concrete placement

Figure 8a shows an overview of the bridge during placement of the joint concrete. The concrete was delivered by truck and then dumped into a large bucket, as shown in Figure 8b. A crane then lifted the bucket over the joint, and the concrete was dispensed (see Figure 8c).

Figure 8d shows the total workforce used for the joint completion. Only four people were used to pour concrete during the 3 hour and 40 minute period. As shown in Figure 8d, one person controlled the bucket, two workers utilized the vibrator, and another person completed the surface finishing. One senior construction engineer provided continuous oversight of the work. In general, it was demonstrated that special skills and equipment beyond what is typical for constructing other bridge types were not required to complete the new longitudinal joint design.

The innovative joint was successfully completed on the bridge. It was demonstrated that the use of rebar couplers is feasible in the field. The placement of the joint concrete went smoothly with a small crew and no special training.

CHAPTER 3. EARLY-AGE PERFORMANCE MONITORING

The results from the Phase I work (Phares 2017, Liu 2018) indicated that cracking tends to initiate during the early age of the joint concrete. For this reason, the early-age joint behavior was closely monitored for the first seven days after construction.

3.1 Instrumentation Design

The early-age joint behavior was monitored with a focus on the bridge's transverse behavior, since the Phase I study indicated that most of the cracking in the joint or debonding at the interface forms in the longitudinal direction. Figure 9 shows the instrumentation plan for early-age monitoring. Two joints were selected for the instrumentation: Joint 1 and Joint 4. In total, 24 vibrating wire strain gauges were utilized, with 16 embedded in the box girders and 8 embedded in the joints.
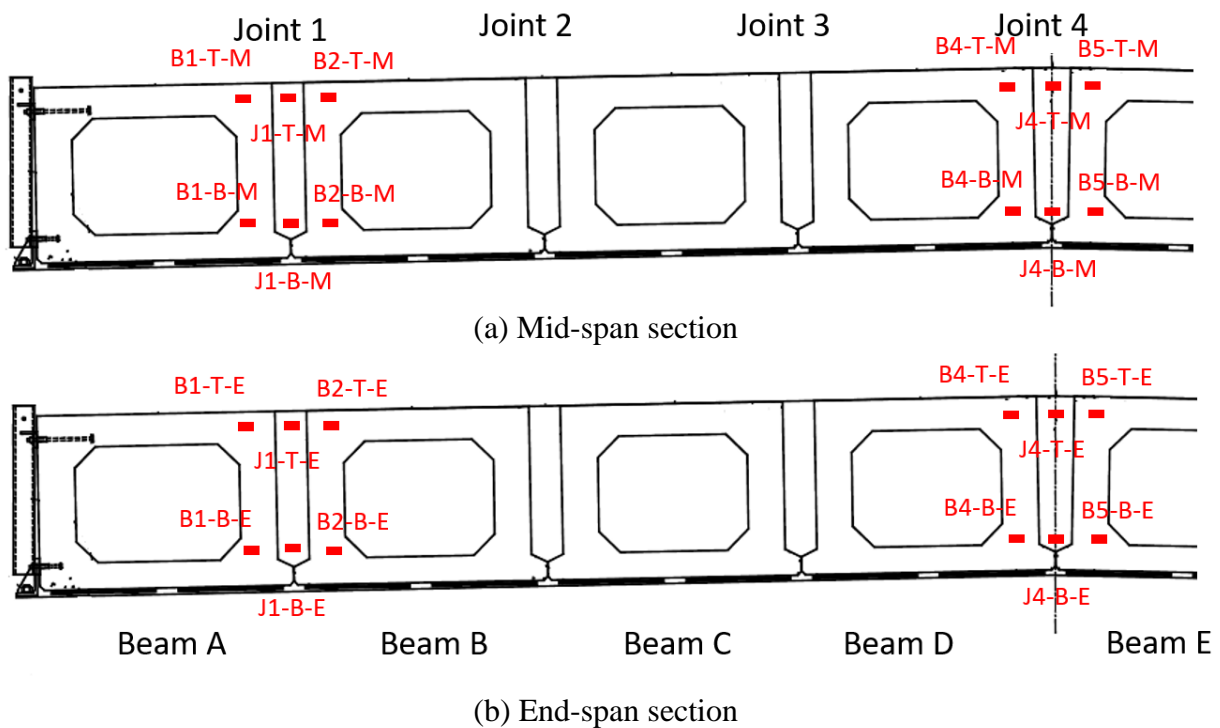

(a) Mid-span section

(b) End-span section

Figure 9. Early-age monitoring instrumentation plan

This instrumentation plan was configured such that the data could be used to study and report on the condition and behavior of the bridge during the early age of the joint material. Strain in the box girders and longitudinal joints is induced by early-age changes in the material's volume and temperature. Vibrating wire strain gauges were placed at the top and near the bottom of the girders and joints under observation.

13

Figure 10 shows the locations of the strain gauges relative to the reinforcement in the box girders.
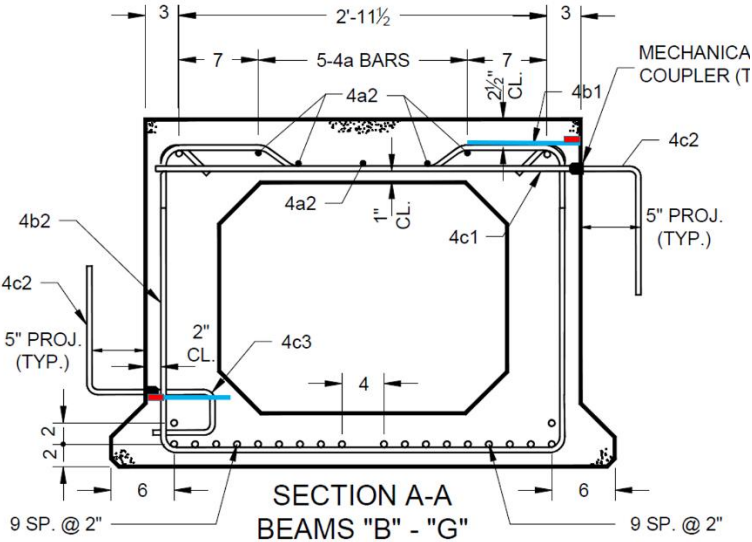

Figure 10. Strain gauge locations in the box girders

Considering the limited timeframe and access during box girder fabrication at the precast plant and completion of the joint in the field, each of the strain gauges (red rectangles in Figure 10a) was attached to a piece of steel rebar (blue lines in Figure 10a, photograph in Figure 11a) and then installed in its position within the girder. Figure 11b and Figure 11c show the strain gauges embedded in a box girder at the top and bottom, respectively. After placement of the box girder concrete, all of the strain gauges in the girders were tested to ensure that they were operational (Figure 11d). The results indicated that they were working properly.

(a) Strain gauge attached to a piece of rebar

(b) Strain gauge at the top of a box girder

(c) Strain gauge at the bottom of a box girder

(d) Testing of the strain gauges

**Figure 11. Embedded strain gauges in a box girder**

The strain gauges in the joints were placed using a similar approach. Figure 12a and Figure 12b show the gauges embedded in a joint near the top and bottom, respectively.

(a) Strain gauge placed at the top of a joint   (b) Strain gauge placed at the bottom of a joint

Figure 12. Embedded strain gauges in a longitudinal joint

All of the strain gauges were connected to the Campbell Scientific CR1000 data logger, as shown in Figure 13a, and the whole data acquisition system was powered by a solar panel, as shown in Figure 13b.
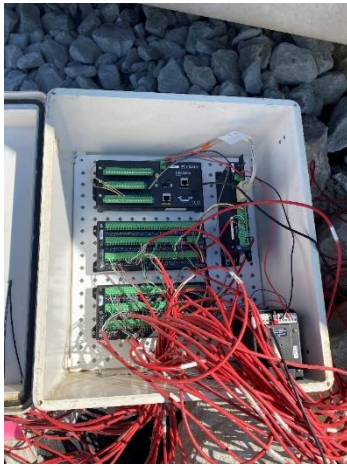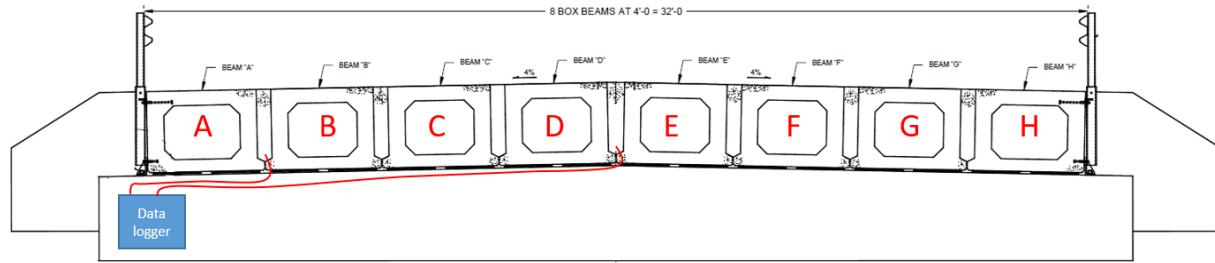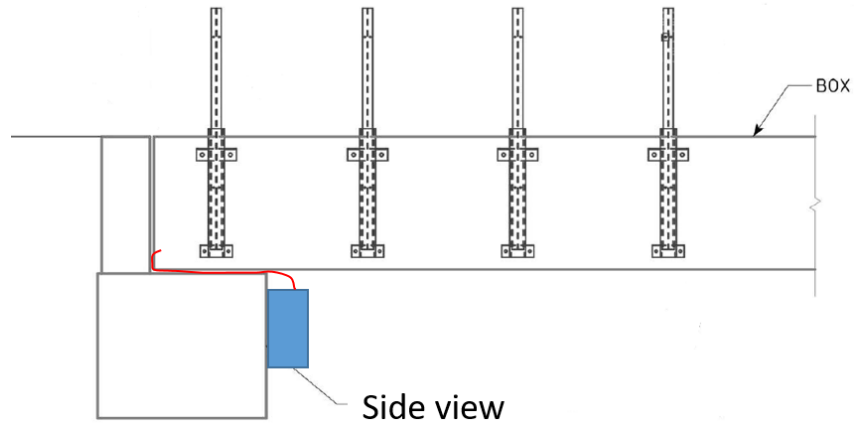

(a) Data logger   (b) Solar panel

Figure 13. Data acquisition system

The data logger and the solar panel were placed on the bank by the north abutment, as shown in Figure 14.

(a) Bridge cross-section view (looking north)

(b) Elevation view

Figure 14. Data logger location

3.2 Monitoring Results

Temperature and strain data were collected during the early-age monitoring. Each vibrating wire strain gauge was equipped with an embedded thermistor. The data collected from this thermistor were used to complete the temperature correction on the strain data and establish a temperature field for each instrumentation section. The field-captured temperature and strain data are presented and discussed in Sections 3.2.1 and 3.2.2.

Data collection started immediately after joint concrete placement at 12:20 p.m. on October 7, 2020, and ended when the joint was seven days old. Data were collected at a frequency of 10 minutes.

3.2.1 Temperature Data

Figure 15 shows the temperatures measured from the vibrating wire strain gauges embedded in the box girders. See Figure 9 for the gauge locations.
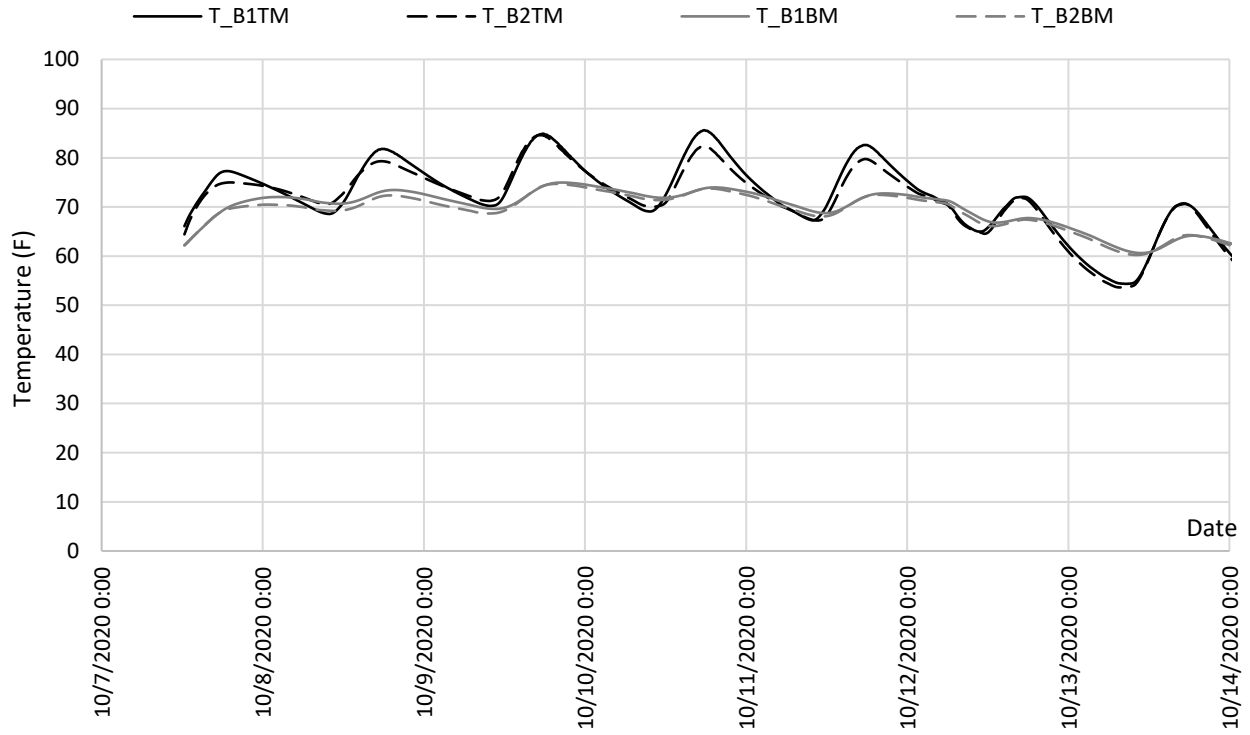
(a) Temperature data from gauges B1TM, B2TM, B1BM, and B2BM
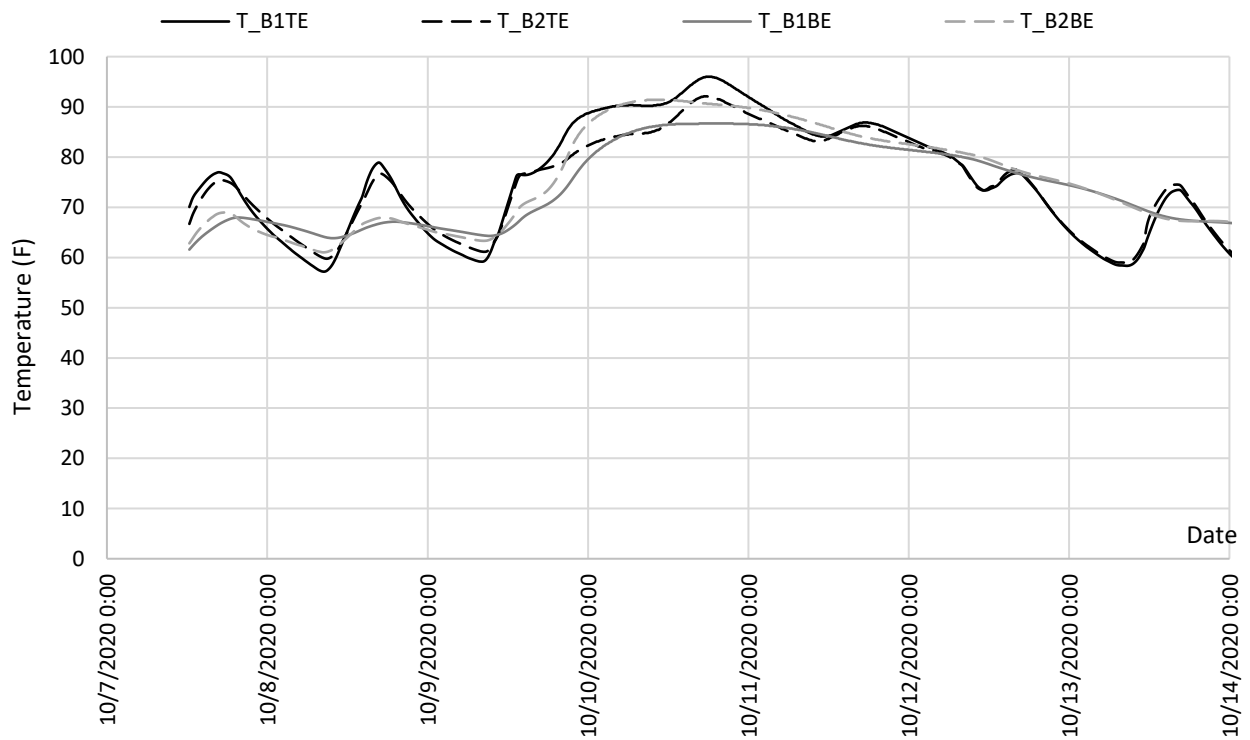
(b) Temperature data from gauges B1TE, B2TE, B1BE, and B2BE
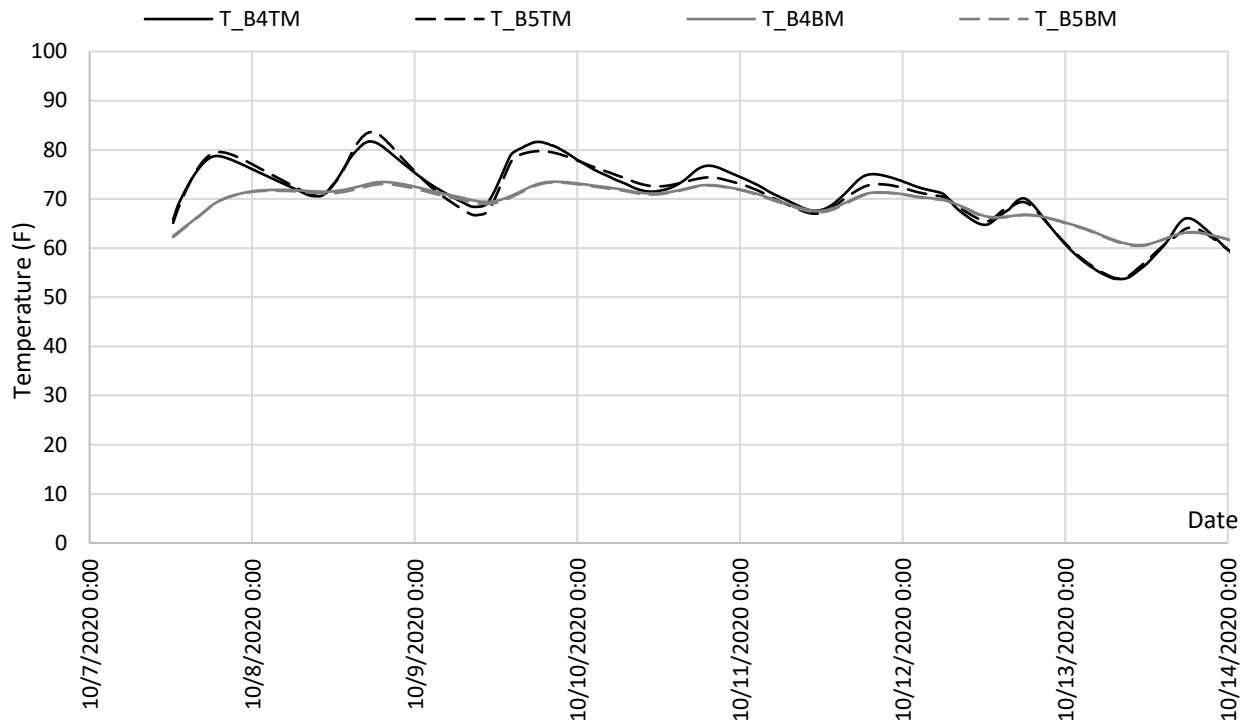
(c) Temperature data from gauges B4TM, B5TM, B4BM, and B5BM

(d) Temperature data from gauges B4TE, B5TE, B4BE, and B5BE

Figure 15. Early-age girder temperature

Figure 15a and Figure 15c show the temperature data measured at the mid-span. The gauges near both the top and bottom of the girders followed a typical daily temper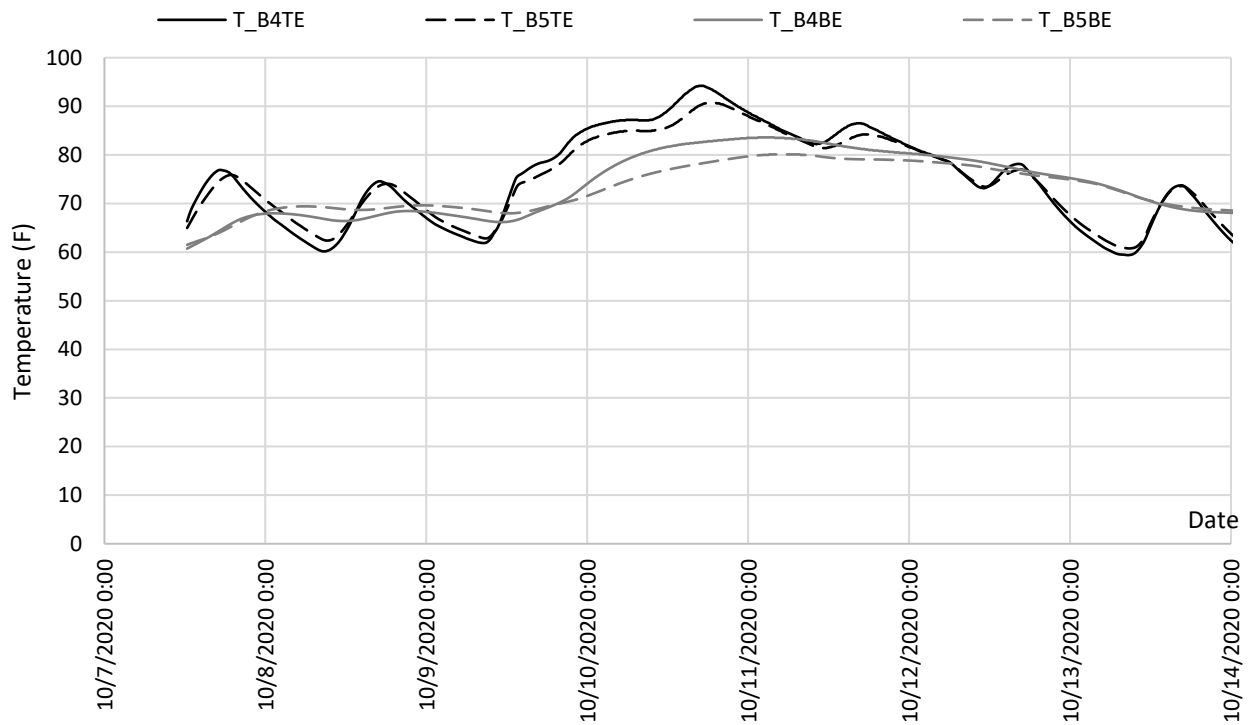ature cycle during the first seven days of the joint age, with higher temperatures in the daytime and lower temperatures at night. It was also observed that the temperature variation between highs and lows near the top of the girders was approximately 15ºF, while the variation near the bottom of the girders was about 6ºF. During the daytime, a 10ºF temperature gradient was captured through the depth of the box girders.

Figure 15b and Figure 15d show the temperature data collected at the end-span. The results show that the temperatures near the end of the span followed the daily temperature cycle during the first two days, and a temperature increase of about 10ºF occurred on the third day (October 9, 2020). After communicating with the field engineer, this temperature increase was found to be induced by the heat of hydration from the placement of the north abutment concrete. Note that the effect from the placement of the abutment concrete was not considered during the design of the innovative joint and was never tested in laboratory conditions.

Figure 16 shows the temperature data collected from the gauges embedded in the longitudinal joints. The data from the gauges at the mid-span showed results similar to those of the gauges embedded in the box girders. Seven complete daily temperature cycles were measured. However, the vertical temperature gradient during the first two days was minimal. This is because the heat of hydration of the joint concrete increased the temperature of the joints. The data from the gauges at the end-span also showed a temperature increase on the third day after the abutment concrete was placed.
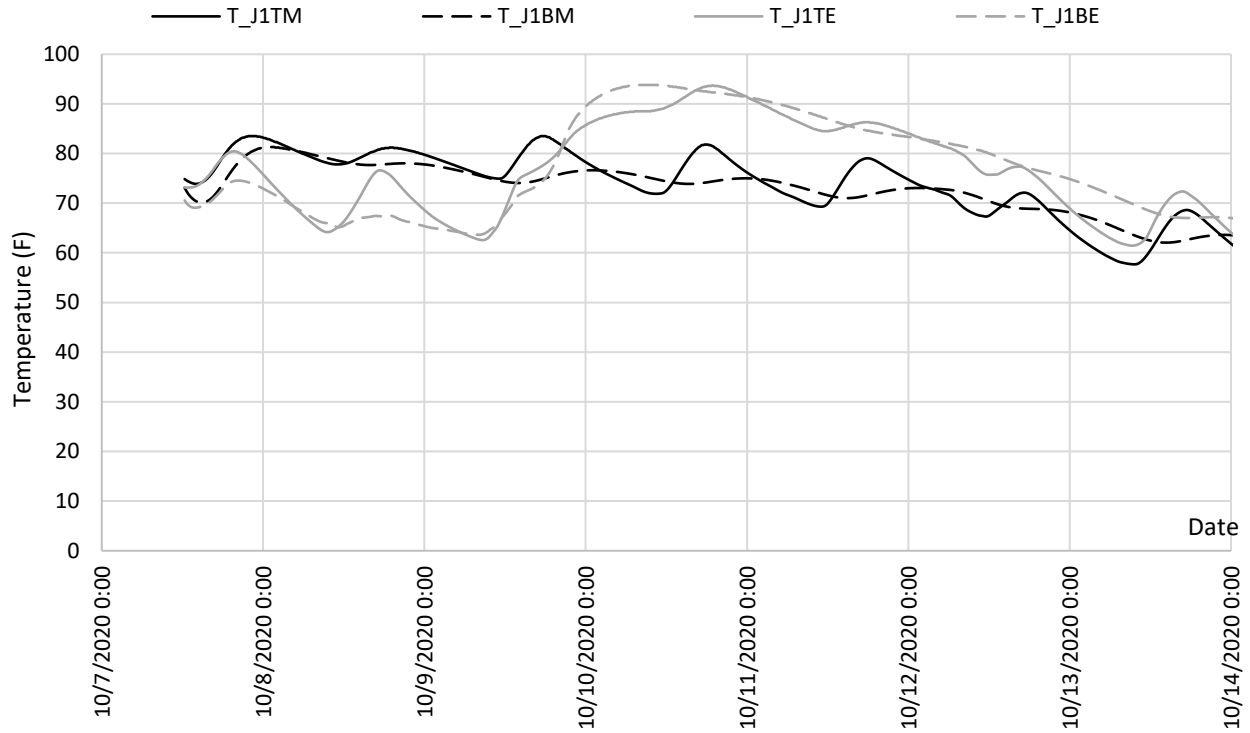
(a) Temperature data from gauges J1TM, J1BM, J1TE, and J1BE
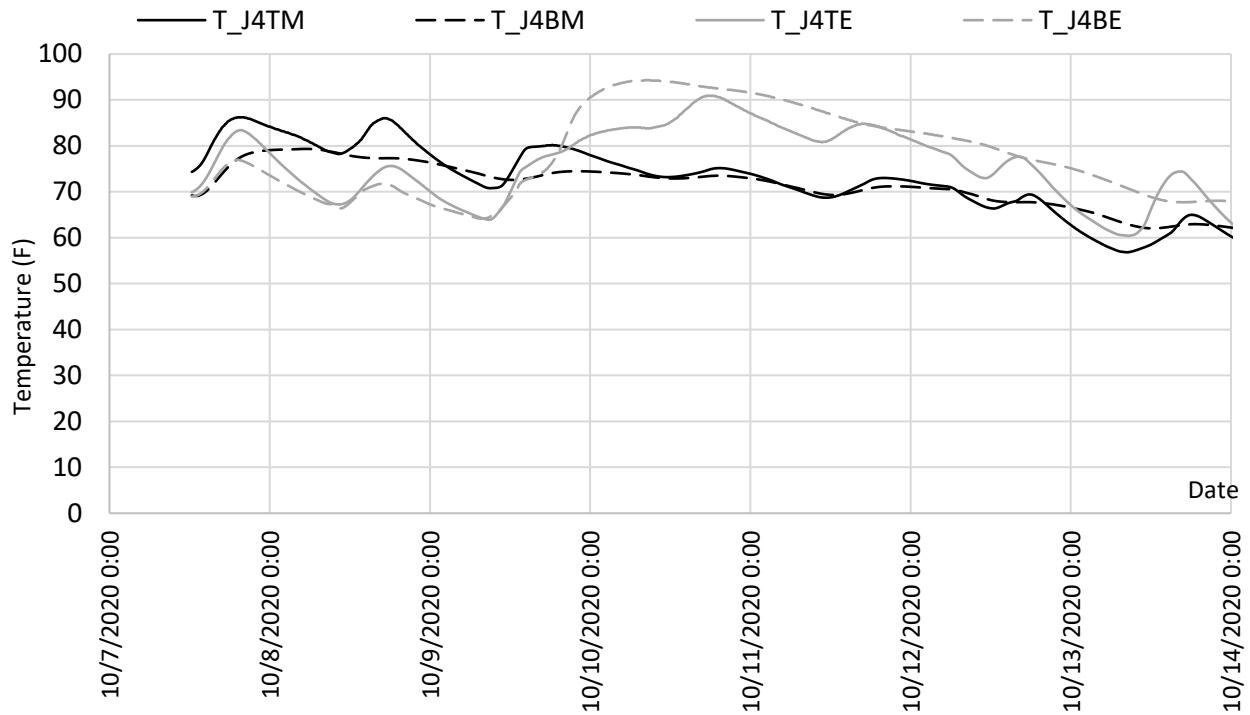
(b) Temperature data from gauges J4TM, J4BM, J4TE, and J4BE

Figure 16. Early-age joint temperature

3.2.2 Strain Data

All of the strain gauges were placed to measure strain in the transverse direction of the bridge. The strain data were corrected for temperature using the temperature data for each gauge.

Figure 17 shows the strain development in the box girders during the first seven days after placement of the joint concrete. In general, all of the strain measured in the girders indicates a small tensile force (less than 20 microstrain). This indicates that the daily temperature change did not induce a significant effect on the box girders.
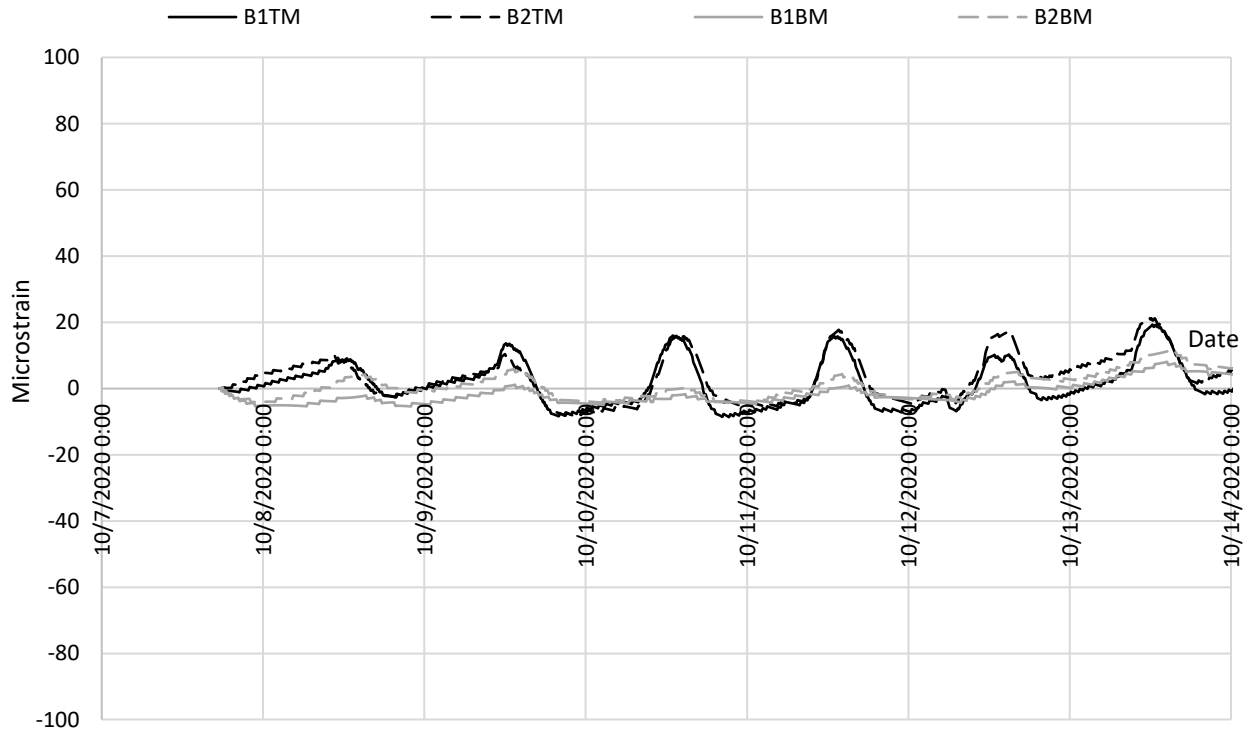
(a) Strain data from gauges B1TM, B2TM, B1BM, and B2BM

(b) Strain data from gauges B1TE, B2TE, B1BE, and B2BE
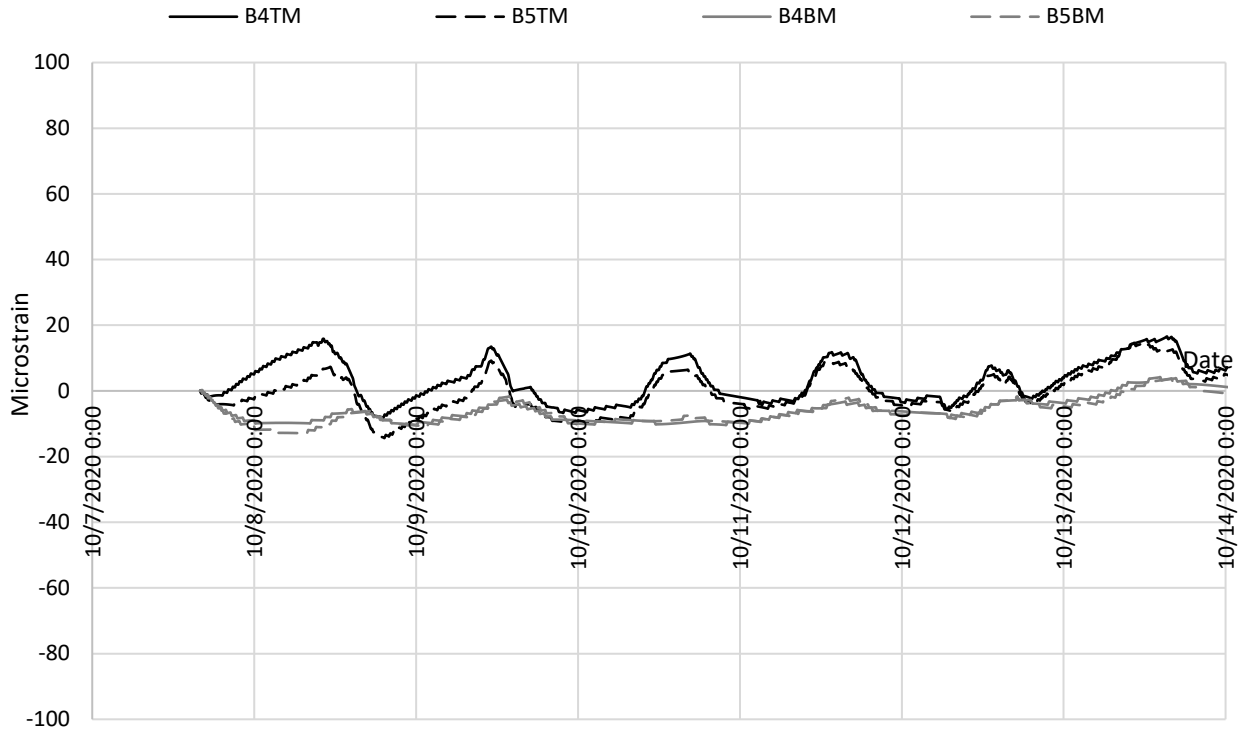
(c) Strain data from gauges B4TM, B5TM, B4BM, and B5BM
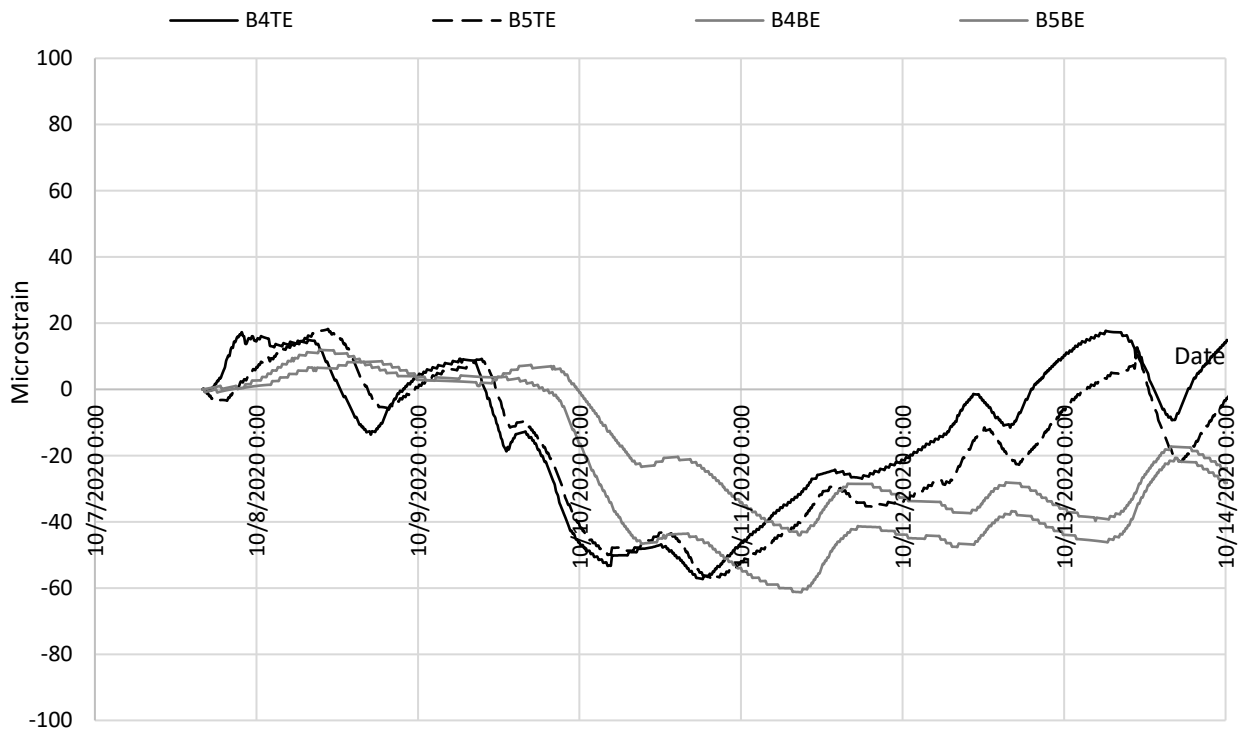
(d) Strain data from gauges B4TE, B5TE, B4BE, and B5BE

Figure 17. Early-age girder strain development

The strain data results at mid-span (Figure 17a and Figure 17c) indicate that the girders were more sensitive to the daytime temperature increases when the top surface was directly exposed to sunlight. The strain change at the bottom of the girders was minimal in comparison.

The strain data results from the end-span are presented in Figure 17b and Figure 17d. It was found that the construction of the abutment had a positive effect on the beam end behavior and reduced the transverse strains. This is likely a result of the shrinkage of the integral abutment during the first few days after placement of the abutment concrete, which provided transverse restraint to the beam ends.

Figure 18 shows the strain data results from the longitudinal joints. Similar to the findings from the Phase I work (Phares 2017), an initial increase of 50 to 300 microstrain was captured during the first 24 hours after joint placement. This tensile force was induced by the Type K cement in the joint material and is desired to create compression at the joint-to-girder interface (Liu and Phares 2019, Liu and Phares 2020, Liu et al. 2020). A comparison of the results from Joints 1 and 4 shows that greater expansion of the joint material occurred in Joint 1.
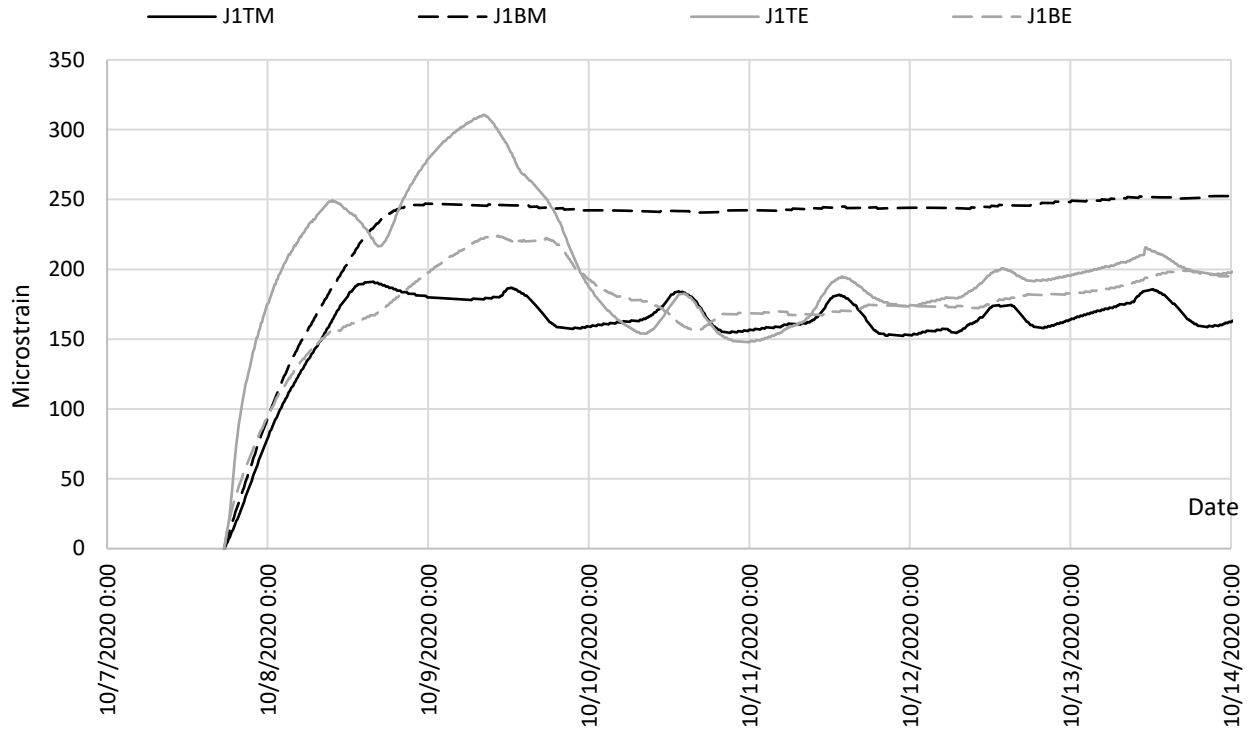
(a) Strain data from gauges J1TM, J1BM, J1TE, and J1BE
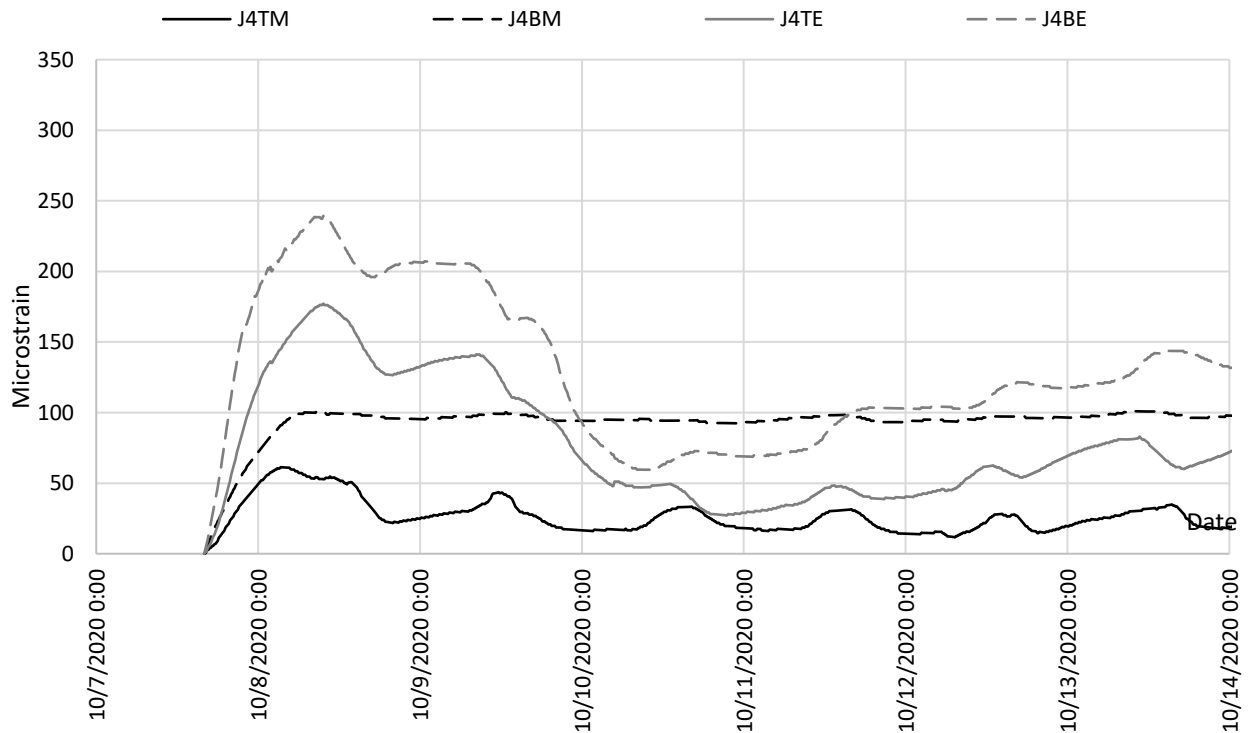
(b) Strain data from gauges J4TM, J4BM, J4TE, and J4BE
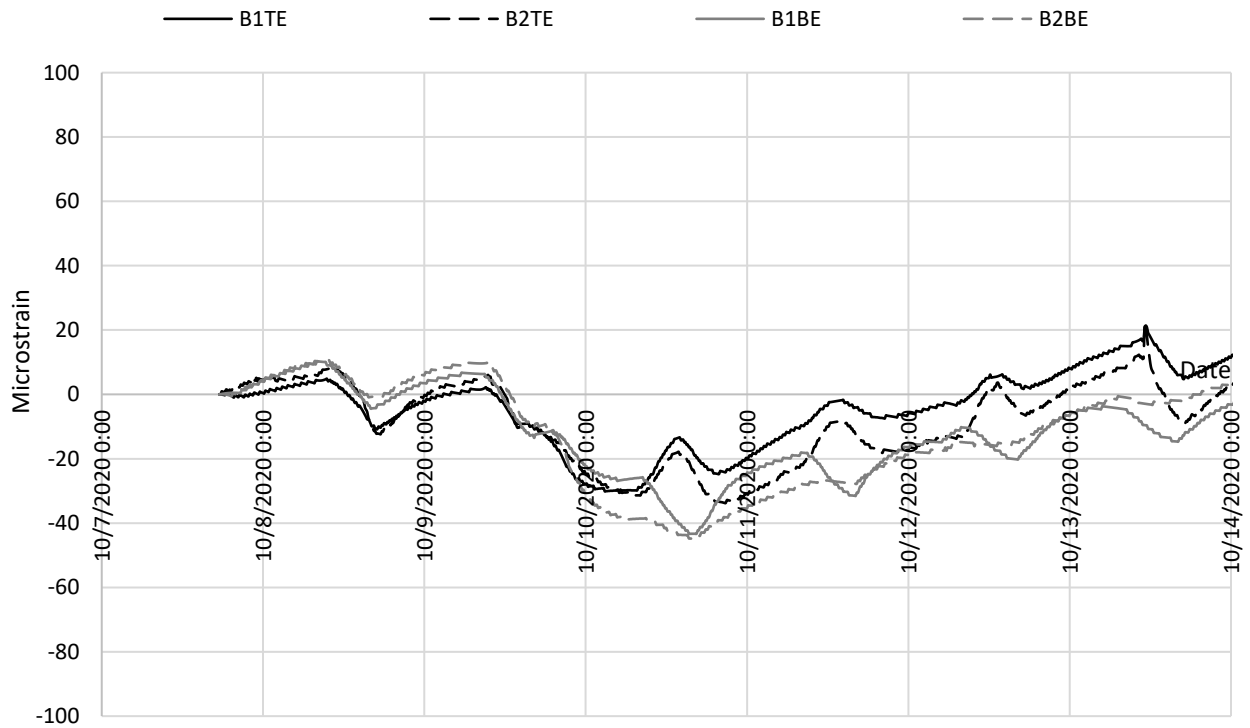
Figure 18. Early-age joint strain development

Similar to the strain data collected from the box girders, the strain measured at the ends of the joints was also affected by the construction of the abutment. This effect is also positive and reduces the transverse strain at the ends of the joints.

3.3 Material Property Tests

In order to perform a qualitative evaluation of the joint concrete, multiple material property tests were conducted with a focus on capturing the time-dependent compressive strength, splitting tensile strength, and self-volume change (expansion). Concrete samples were cast for the material used in Joints 1 and 4, where the strain gauges were located, to account for any potential material differences due to delivery in separate trucks. See Figure 7 for joint material placement details.

Shrinkage testing was conducted following the methods prescribed in ASTM C157, Standard Test Method for Length Change of Hardened Hydraulic-Cement Mortar and Concrete. This test method determines changes in length in hardened hydraulic cement mortar and concrete that are produced by causes other than externally applied forces and temperature changes. For each truck material (Truck 1 and Truck 2), three specimens (shown in Figure 19a) were cast and then cured at room temperature, or about 24°C (75°F), with 100% humidity. For each test, the mold was removed 6 hours after pouring, and the first data were measured immediately after removal of the mold. Shrinkage data were collected at 12 hours, 1 day, 2 days, 3 days, 7 days, 14 days, and 28 days.

The average shrinkage of the concrete from each truck is shown in Figure 20a. For both trucks, values of 200 to 310 microstrain were measured during the first 24 hours. These values match the findings from the field-measured strain data, where most of the concrete expansion occured during the first 24 hours after placement. In addition, the magnitude of the expansion (310 microstrain in Joint 1 and 200 microstrain in Joint 4) shows agreement with the expansion measured in the field joints, where more expansion occurred in Joint 1.

Compressive strength was tested following the methods prescribed in ASTM C39, Standard Test Method for Compressive Strength of Cylindrical Concrete Specimens, and splitting tensile strength was tested following the methods prescribed in ASTM C496, Standard Test Method for Splitting Tensile Strength of Cylindrical Concrete Specimens. For each truck of concrete, 24 concrete cylinders with a diameter of 4 in. and a length of 8 in. were cast, with half of the cylinders used for the compressive strength tests (Figure 19c) and the other half used for the splitting tensile strength tests (Figure 19d). In order to capture the time-dependent material properties, the compressive strength and the tensile strength were tested when the material age was 6 hours, 1 day, 7 days, and 28 days.

Figure 20b and Figure 20c show the material test results for compressive strength and tensile strength, respectively. The results show that the concrete from both trucks had similar compressive strength values on the 28th day of 5.2 to 5.8 ksi. These values are higher than the required compressive strength (4 ksi) for the joint material per the construction documents. For the tensile strength, similar strength values of 0.4 ksi on the 28th day were measured for the

concrete in both trucks. The time-dependent behavior of the material indicated that Type K cement concrete underwent a significant strength increase during the first 24 hours.

(a) Concrete samples for shrinkage testing

(b) Shrinkage test machine
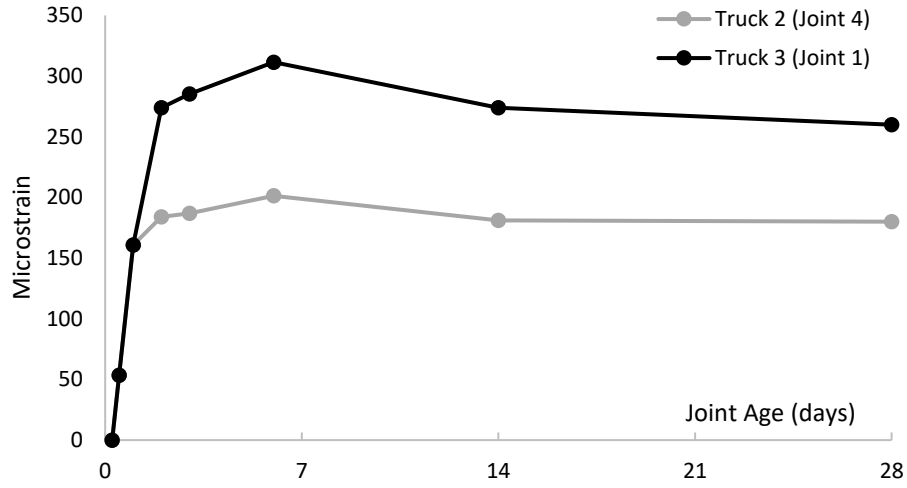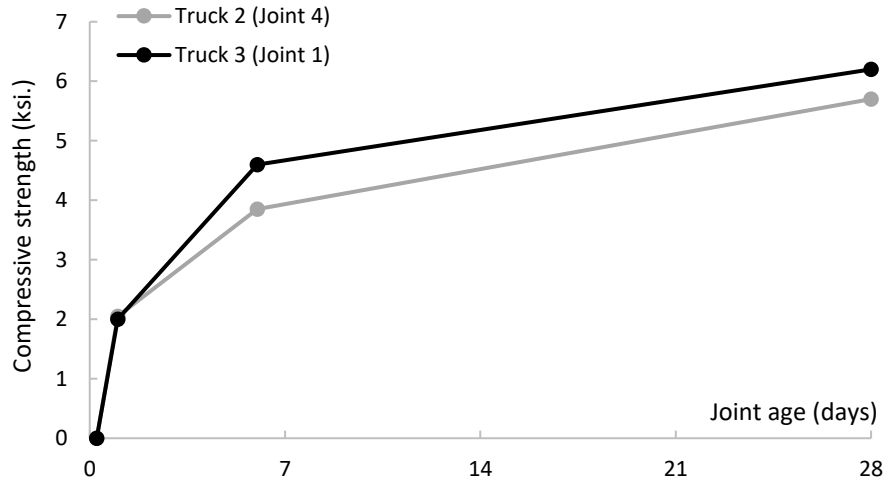

(c) Compressive strength test
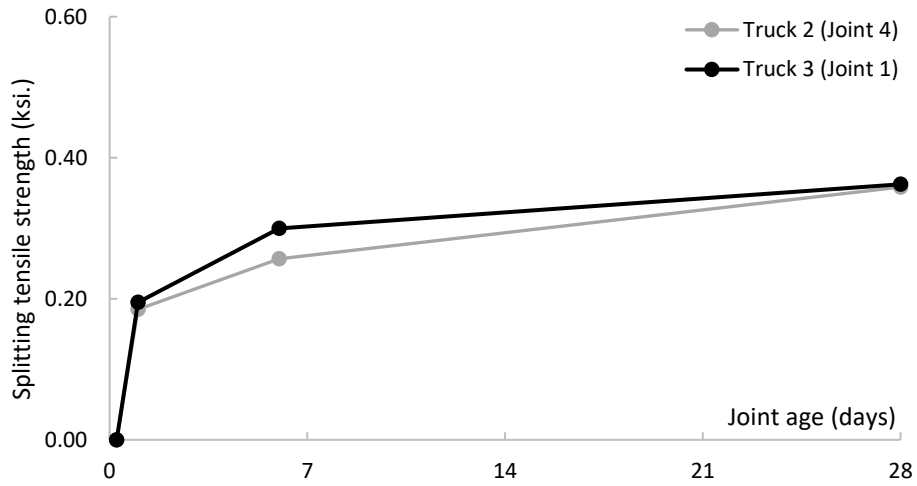

(d) Splitting tensile strength test

Figure 19. Material property tests

(a) Shrinkage

(b) Compressive strength

(c) Splitting tensile strength

Figure 20. Material property test results

CHAPTER 4. LONG-TERM PERFORMANCE EVALUATION

The main objective of the long-term performance evaluation was to investigate the performance of the longitudinal joints with respect to crack resistance and transverse load distribution. To complete this objective, three live load field tests and four visual deck/joint concrete crack inspections were completed.

The live load tests were conducted with a focus on identifying any changes in lateral load distribution characteristics over time. The bridge was opened to traffic in early November 2020, and the first load test was conducted on November 18, 2020. The second and third tests were performed on October 7, 2021, and August 16, 2022, respectively, approximately one and two years after construction. During the live load tests, a data acquisition system was used to collect strain and displacement data from the bridge at specific designated locations so the data could be analyzed and compared to determine any differences in behavior. Specifically, any changes in lateral live load distribution characteristics were of particular interest.

The visual inspections principally focused on assessing the condition and performance of the joints, with particular attention paid to the development of any cracking.

4.1 Live Load Tests

Three live load tests were conducted throughout the project in November 2020, October 2021, and August 2022. To aid in the interpretation of the data, the research team used controlled live load testing, where a known load crosses the bridge at predetermined locations. The live load was a three-axle truck (with wheel spacing depicted in Figure 21) with a total weight of 64,630 lb. The truck was driven across the bridge from north to south at a crawl speed (approximately 5 mph) to induce a pseudo-static load on the bridge.
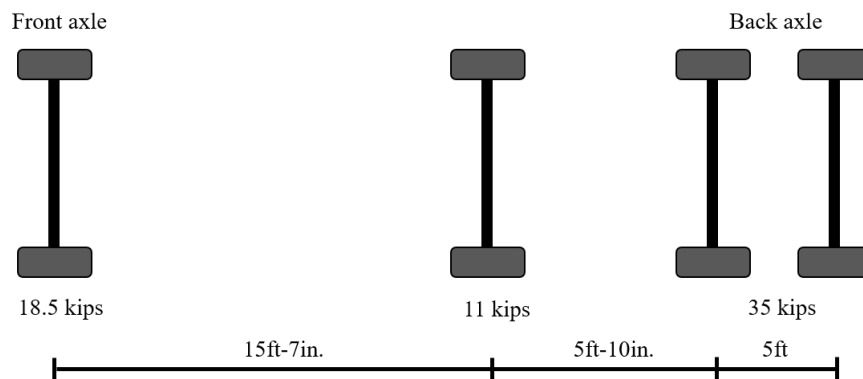
Figure 21. Truck configuration and axle loads

Considering that the bridge had a limited width of 32 ft and only two traffic lanes, three load cases (LCs) were performed during each load test. Figure 22 shows the truck's position for each LC relative to the box girders in the bridge's transverse direction. For LC1, the truck was driven

with the centerline of the passenger's side wheel offset by 2 ft from the bridge centerline. For LC2, the truck was driven with the centerline of the truck on the centerline of the bridge. For LC3, the truck was driven with the centerline of the driver's side wheel offset by 2 ft from the bridge centerline.
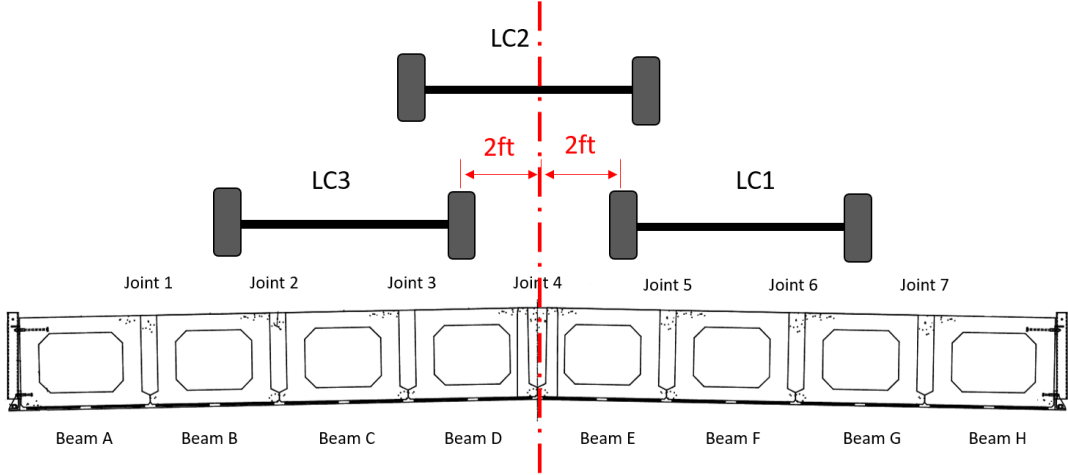
Figure 22. Live load cases

During testing, the strain data were marked at 10 ft intervals as the truck traveled longitudinally down the bridge. Marking the data allowed the timestamp to be converted to truck position and ensured that the collected time-domain data matched the physical truck position. Figure 23 shows one of the live load tests being completed.

Figure 23. Live load test

4.2 Instrumentation Plan

Before the beginning of the live load tests, the bridge was instrumented with eight BDI strain gauges and six displacement transducers. The instrumentation plan was designed with the goal of

31

collecting sufficient data to qualitatively evaluate the load distribution and any changes in performance that might have occurred between tests.

Figure 24 shows the instrumentation plan used during the live load tests. All of the gauges were installed at mid-span on the bottom surface of the superstructure. One BDI strain gauge was attached at the middle of the bottom surface of each box girder (SA to SH in Figure 24) to measure the strain in the bridge's longitudinal direction. Three displacement transducers (DA, DD, and DH) were placed underneath Beam A, Beam D, and Beam H to measure the vertical displacement at the mid-span. Another three displacement transducers (DAB, DBC, and DCD) were placed in the bridge's transverse direction to measure any separation between the adjacent girders.

Figure 24. Instrumentation plan for live load tests (bottom surface of superstructure)

Figure 25 shows photographs of the on-site instrumentation placement.

Figure 25. Live load test instrumentation placement
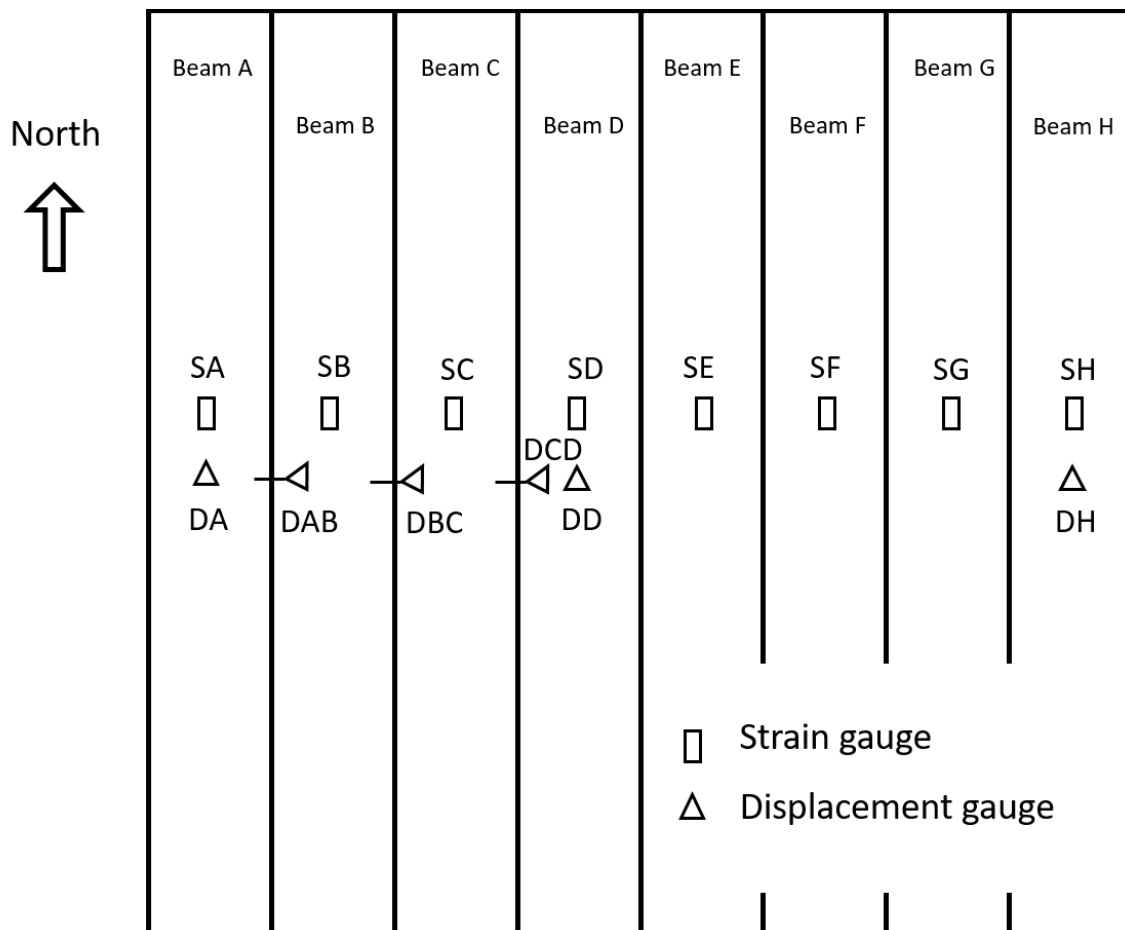
4.3 Test Results

In this section, the data collected from each year's load test are analyzed and presented with respect to the load distribution characteristics.

Equation 1 was used to calculate the load distribution for each box girder.

$$LDF_i = \varepsilon_i \Big/ \sum_{i=A}^{H} \varepsilon_i \tag{1}$$

where ε_i is the strain collected from the ith box girder and LDF_i is the load distribution factor (LDF) for the ith box girder.

Utilizing the strain values to estimate the load distribution is valid because the load distribution reflects the distribution of moment over the girders and because the longitudinal strain at the bottom of the mid-span is linearly related to the moment, as shown in Equation 2.

$$\varepsilon_i = \frac{M_i y}{EI} \tag{2}$$

where M_i is the moment carried by the ith box girder, E is the Young's modulus of the material, I is the moment of inertia, and y is the distance from the neutral axis to the strain measurement location.

The vertical displacement data were used to determine the overall general response and symmetry of performance. Additionally, the mid-span displacement values were compared to the maximum recommended displacement values prescribed by the American Association of State Highway and Transportation Officials (AASHTO) *Load and Resistance Factor Design Bridge Design Specification* (LRFD BDS), Section 2.5.2.6.2. The horizontal displacement between

girders was evaluated at three locations, and the results showed that no relative movement was measured at those locations. Therefore, the horizontal displacement data are not presented herein.

4.3.1 2020 Load Test

For brevity, despite the fact that a total of three load cases were performed, only the complete data from LC3, when the driver's side wheel of the truck was positioned 2 ft west of the centerline of the bridge, are presented as an example. The data from the other two load cases were also processed, and the results do not change the overall evaluation of performance.

Figure 26 shows the vertical displacement at mid-span from LC3. All three displacement transducers (Girders A, D, and H) show a similar magnitude of displacement ranging from 0.08 to 0.10 in, with the westernmost displacement being the greatest. This indicates that the load distribution is fairly uniform across the bridge, assuming approximately uniform transverse stiffness of the box girder assembly. Overall the structure is rather stiff, considering that the maximum displacement of approximately 0.10 in. is smaller than the maximum recommended AASHTO LRFD BDS value of 1.05 in., calculated as 1/800th of the bridge length (70 ft).
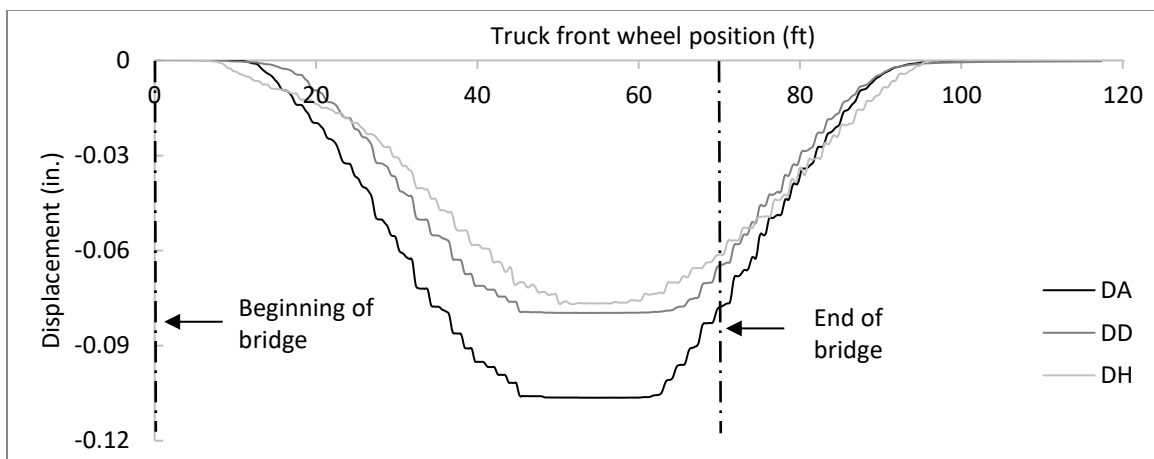

Figure 26. Vertical displacement results from LC3 (2020)

Figure 27 shows the strain data collected during LC3. The maximum strain ranges from 15 to 34 microstrain. In general, this strain is small compared to the concrete cracking strain of 132 microstrain as calculated by $7.5 \sqrt{f_c'}/57{,}000 \sqrt{f_c'}$ (ACI Committee 318 2011).

Figure 27. Strain results from LC3 (2020)

Figure 28 shows the peak strain distribution in the transverse direction for all three load cases, which provides a better illustration of the load distribution. The results indicate that all girders are engaged and resisting load regardless of the truck's transverse position. The maximum strain from all three LCs is about 38 microstrain, which is not significant for prestressed concrete girders.
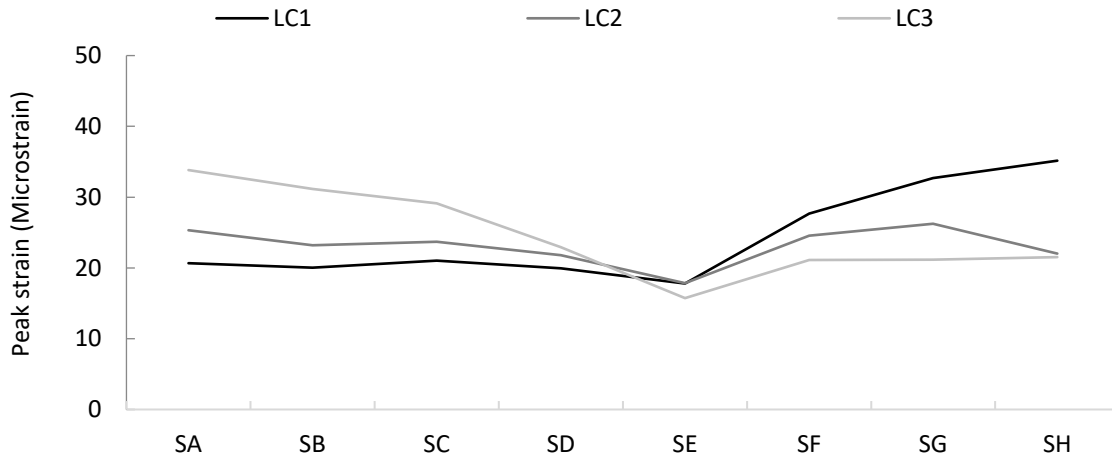
Figure 28. Peak strain distribution in the transverse direction (2020)

The load distribution factors for each girder were calculated utilizing the field-collected strain data and equation (1). This calculation assumes that the stiffness of all girders is the same. Table 2 shows the load distribution factors from the 2020 test. The maximum calculated LDF is 0.17 for the interior girder and 0.18 for the exterior girder. Both cases occurred during LC1, when the centerline of the passenger's side wheel was offset by 2 ft from the bridge centerline.

Table 2. Load distribution factors from 2020 load test

	A	B	C	D	E	F	G	H
LC1	0.11	0.10	0.11	0.10	0.09	0.14	0.17	0.18
LC2	0.14	0.13	0.13	0.12	0.10	0.13	0.14	0.12
LC3	0.17	0.16	0.15	0.12	0.08	0.11	0.11	0.11

4.3.2 2021 Load Test

Consistent with Section 4.3.1, only the complete data from LC3, when the driver's side wheel of the truck was positioned 2 ft west of the centerline of the bridge, are presented in this section as an example. The data from the other two load cases were also processed, and the results do not change the conclusions.

Figure 29 shows the vertical displacement at mid-span from LC3. All three displacement transducers (Girders A, D, and H) show a similar magnitude of displacement ranging from 0.05 to 0.09 in., which, as in the first load test, indicates that the load distribution is fairly uniform across the bridge, assuming approximately uniform transverse stiffness of the box girder assembly. Additionally, the displacement data show that no appreciable change in the structure occurred between the first and second load tests. The maximum displacement captured by gauge DH is about 0.09 in., which is only slightly less than the maximum displacement (0.10 in.) captured during the 2020 load test (see Figure 26). It is possible that there was a slight increase in structural stiffness due to the aging concrete. However, the difference in maximum deflection is deemed insignificant.

Figure 29. Vertical displacement results from LC3 (2021)

Figure 30 shows the strain data collected during LC3. The maximum strain ranges from 15 to 31 microstrain, which is only slightly less than the measured strain range in 2020 (15 to 34

microstrain). In general, this strain is small compared to the concrete cracking strain of 132 microstrain as calculated by $7.5\sqrt{f'_c}/57{,}000\sqrt{f'_c}$ (ACI Committee 318 2011).
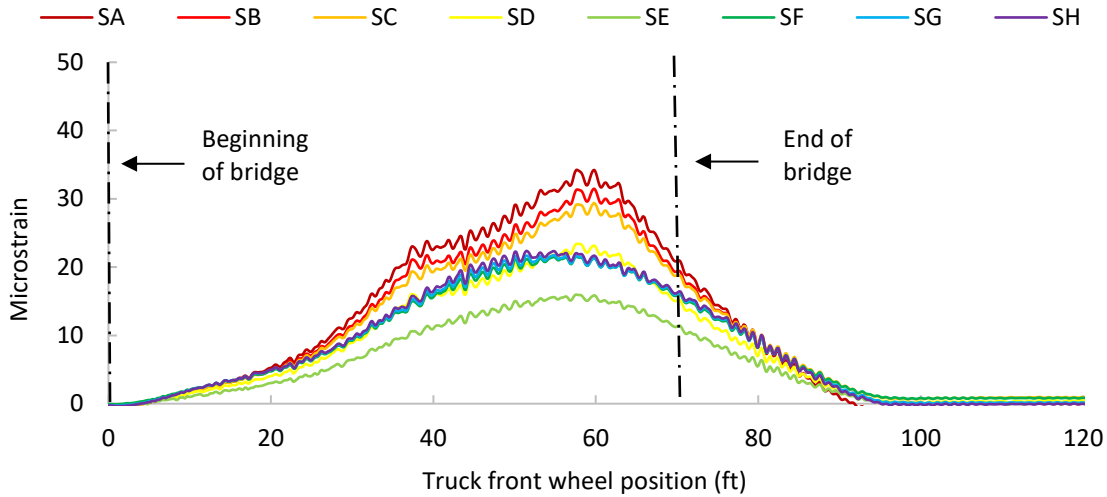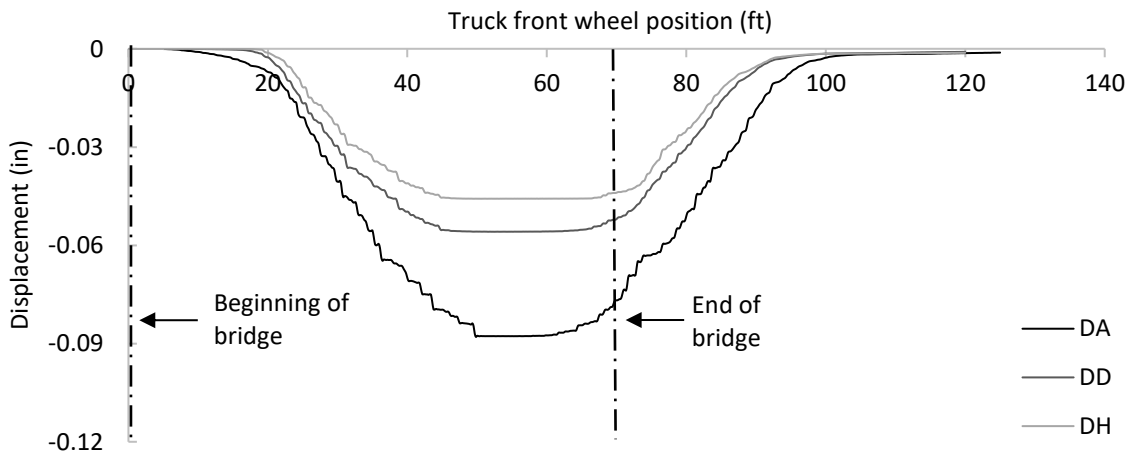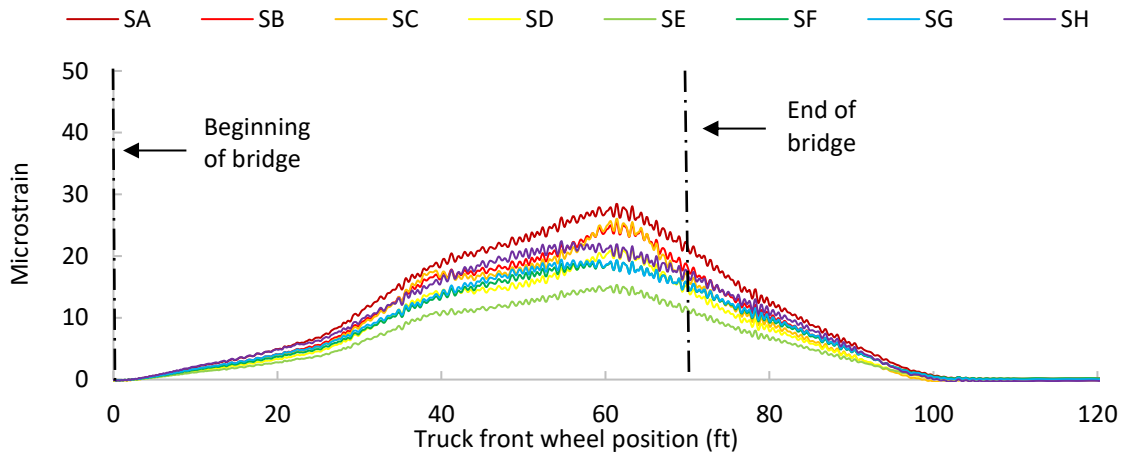

Figure 30. Strain results from LC3 (2021)

Figure 31 shows the peak strain distribution in the transverse direction for all three load cases. The results indicate that all girders are engaged in carrying the load regardless of the truck's transverse position. No significant load concentration (on a single beam) was apparent by observation. The maximum strain from all three LCs is about 31 microstrain, which is not significant for prestressed concrete girders.
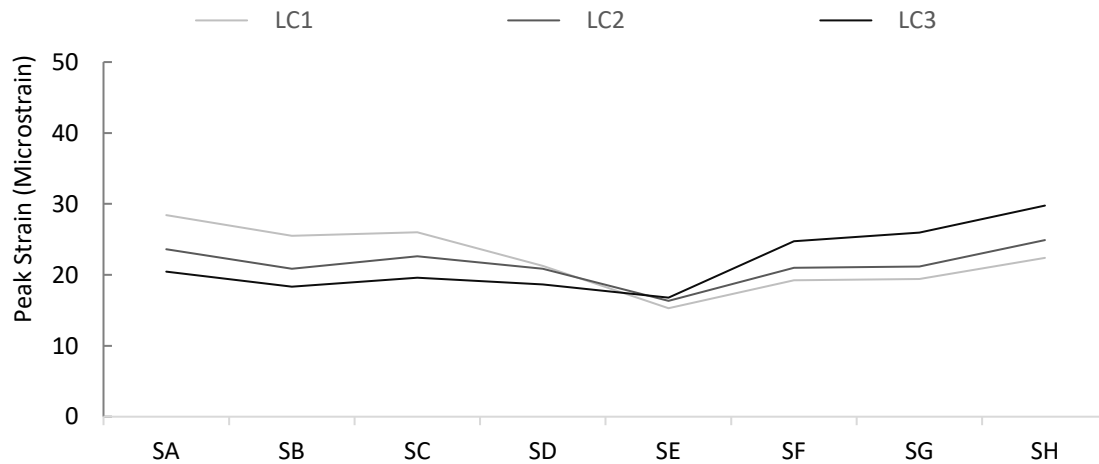
Figure 31. Peak strain distribution in transverse direction (2021)

Table 3 shows the load distribution factors for each girder from the 2021 load test calculated utilizing the field-collected strain data and equation (1). The maximum LDF is 0.15 for the interior girder and 0.17 for the exterior girder. Both cases occured during LC1, when the centerline of the passenger's side wheel was offset by 2 ft from the bridge centerline. Compared to the results from the 2020 load test, the maximum LDFs are slightly smaller. This may also be

37

a result of increased stiffness due to the aging concrete. Generally, the results indicate that no noteworthy change in structural performance occurred in the joints during the first year in service and that the bridge superstructure remained in overall good condition.

Table 3. Load distribution factors from 2021 load test

	A	B	C	D	E	F	G	H
LC1	0.12	0.11	0.11	0.11	0.10	0.14	0.15	0.17
LC2	0.14	0.12	0.13	0.12	0.10	0.12	0.12	0.15
LC3	0.16	0.14	0.15	0.12	0.09	0.11	0.11	0.13

4.3.3 2022 Load Test

Consistent with Section 4.3.1, only the complete data from LC3, when the driver's side wheel of the truck was positioned 2 ft west of the centerline of the bridge, are presented in this section as an example. The data from the other two LCs were also processed, and the results indicated no significant difference in overall performance.

Figure 32 shows the vertical displacement at mid-span from LC3. All three displacement transducers (girders A, D, and H) show a similar magnitude of displacement ranging from 0.05 to 0.10 in., which is consistent with the results of the previous two load tests and is demonstrative of the load distribution performance of the superstructure. The maximum displacement captured by gauge DH is about 0.10 in., which is similar to the maximum displacement values (0.09 to 0.10 in.) measured during the 2020 and 2021 load tests. In every case, the displacement magnitude is well below the recommended maximum prescribed in the AASHTO LRFD BDS of 1/800th of the bridge length, or 1.05 in.
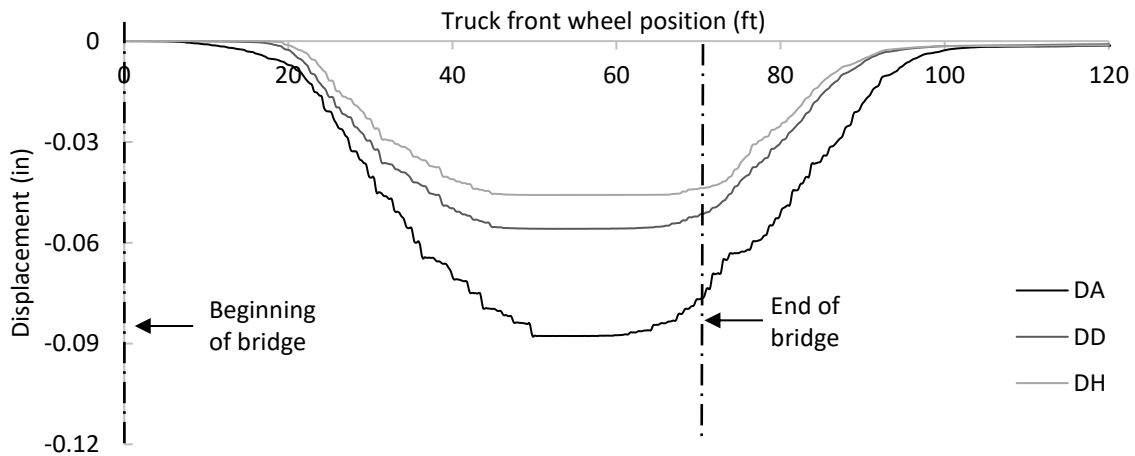

Figure 32. Vertical displacement results from LC3 (2022)

Figure 33 shows the strain data collected from gauges SA to SG during LC3. During the 2022 load test, the strain gauge below Girder H (SH) malfunctioned, and no data were collected from this gauge. The maximum strain ranges from 15 to 29 microstrain, which is consistent with the strain range observed during the 2021 load test (15 to 31 microstrain). As previously noted, these strain values are small compared to the concrete cracking strain of 132 microstrain as calculated by $7.5\sqrt{f_c'}/57{,}000\sqrt{f_c'}$ (ACI Committee 318 2011).

Figure 33. Strain results from LC3 (2022)

Figure 34 shows the peak strain distribution in the transverse direction for all three load cases. Consistent with the results from previous years' load tests, the data indicate that all girders are engaged with respect to load resistance regardless of the truck's transverse position. As in previous load tests, no girders were observed to carry a comparatively high amount of the total load, which further demonstrates the good load distribution in the transverse direction. The maximum strain from all three LCs is approximately 30 microstrain, which is not significant for prestressed concrete girders.
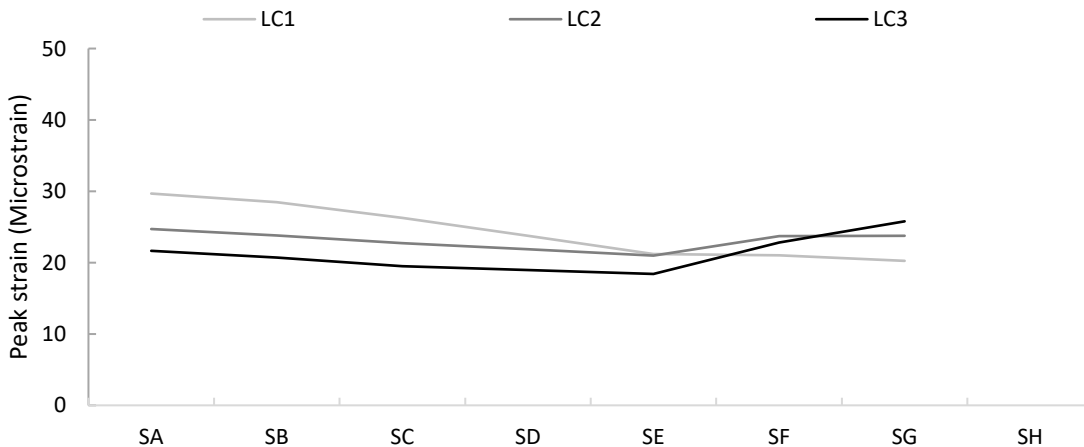

Figure 34. Peak strain distribution in transverse direction (2022)

39

During the 2022 load test, no data were collected from strain gauge SH, which is required to fully determine the live load distribution. Despite this fact, it was decided not to repeat the live load test because the strain and displacement data that were collected and are shown in Figure 32, Figure 33, and Figure 34 indicate no significant change in structural performance in comparison to the previous load tests.

4.4 Visual Inspection

Visual inspections were conducted every six months after the joint concrete placement. Within a few weeks after the joint placement, the bridge was topped with gravel, which can inhibit a full view of the joints. Accordingly, it became challenging in some locations to inspect the full deck for cracks.

The first inspection was conducted in October 2020. The road had not been covered by gravel at this time, and the bridge had not been opened to traffic. A detailed inspection was completed on all joints, and no cracks were observed. Figure 35 shows the top surface during this inspection.

(a) Bridge top surface   (b) Top surface near joint end

Figure 35. Crack inspection – October 2020

The second inspection occurred on May 3, 2021, approximately half a year after the previous inspection. By this time, the deck had been covered with gravel, as shown in Figure 36.

Figure 36. Top surface of the bridge deck – May 2021

The gravel did not allow for a comprehensive inspection of the top surface. However, the research team intentionally chose to complete the inspection on a rainy day to observe any potential water permeation through the joints. The research team observed the bottom side of the bridge during the rain. During this period, the underside of the bridge remained dry and clean, with no evidence of water permeation. The only evidence of leakage through the joints appeared to be that of concrete paste, which is most likely a byproduct of joint construction (see Figure 37).

Figure 37. Paste leakage during initial construction

The third and fourth inspections were conducted on October 6, 2021, and August 16, 2022, respectively. In each case, no additional noteworthy differences in joint condition were observed.

CHAPTER 5. SUMMARY AND CONCLUSIONS

This project demonstrated the field implementation of an innovative longitudinal cast-in-place joint between prestressed, precast concrete box girders. The joint was designed during a previous research phase and included a unique rebar configuration and the use of Type K cement within the concrete mix to limit the volumetric changes that occur as concrete cures. A yet-to-be-constructed bridge in Washington County, Iowa, was selected for this demonstration.

In order to document the construction of the bridge and to evaluate the performance of the joint, the research team observed the casting of the girders in a precast concrete plant and the field construction of the bridge and then conducted a seven-day field monitoring study during the early age of the joint concrete and a long-term evaluation consisting of both live load field tests and visual deck inspections. The live load tests were performed once per year and the deck inspections were performed twice per year from 2020 through 2022.

During the monitoring and field testing tasks, temperature, strain, and displacement data were collected at critical locations and analyzed to evaluate joint performance with respect to crack resistance and load distribution. The conclusions from this field demonstration are as follows:

- The innovative joint sufficiently resists early-age longitudinal joint cracking. Joint cracks seen on another box girder bridge with traditionally constructed joints were not observed in this case.

- The innovative joint sufficiently distributes live loads in the transverse direction. Results of the live load tests indicate that the concrete box girder and joint assembly act nearly monolithically between individual components. Deflection and strain values observed at gauge locations beneath the passing live load truck were not significantly greater than the values observed at gauge locations opposite the truck's location. Overall, the structure has a high stiffness, with deflection values much lower than the maximum recommended deflection limit per AASHTO LRFD BDS.

- The integral abutment of the bridge, which encapsulates the girder ends, positively affects the strain distribution in the innovative joint near the joint ends. The abutment provides restraint in the transverse direction, thereby aiding the resistance to joint cracking.

- After two years in service, the innovative joint remains in very good condition with no observable cracking present. The live load performance has remained relatively unchanged since the joint's initial construction. The innovative joint design, inclusive of a unique rebar configuration and Type K cement, has resulted in a durable and well-performing joint.

REFERENCES

AASHTO. 2020. *AASHTO LRFD Bridge Design Specifications*. American Association of State Highway and Transportation Officials, Washington, DC.

ACI Committee 318. 2011. *Standard AA. Building Code Requirements for Structural Concrete*. American Concrete Institute, Farmington Hills, MI.

Attanayake, U., and H. Aktan. 2008. Issues with reflective deck cracks in side-by-side box beam bridges. 2008 Concrete Bridge Conference, May 4–7, St. Louis, MO.

Dong, H., Y. Li, and T. M. Ahlborn. 2007. Performance of joint connections between decked prestressed concrete bridge girders. 2007 National Bridge Conference, October 19–22, Phoenix, Arizona.

El-Remaily, A., M. K. Tadros, T. Yamane, and G. Krause. 1996. Transverse design of adjacent precast prestressed concrete box girder bridges. *PCI Journal*, Vol. 41, pp. 96–113.

Grace, N. F., E. A. Jensen, and M. R. Bebawy. 2012. Transverse post-tensioning arrangement for side-by-side box-beam bridges. *PCI Journal*, Vol . 57, No. 2, pp. 48–63.

Hanna, K., G. Morcous, and M. K. Tadros. 2011. Adjacent box girders without internal diaphragms or post-tensioned joints. *PCI Journal*, Vol. 56, No. 4, pp. 51–64.

Hansen, J., K. Hanna, and M. K. Tadros. 2012. Simplified transverse post-tensioning construction and maintenance of adjacent box girders. *PCI Journal*, Vol. 57, No. 2, pp. 64–79.

Huckelbridge Jr., A. A., H. El-Esnawi, and F. Moses. 1995. Shear key performance in multibeam box girder bridges. *Journal of Performance of Constructed Facilities*, Vol. 9, No. 4, pp. 271–285.

Lall, J., S. Alampalli, and E. F. DiCocco. 1998. Performance of full-depth shear keys in adjacent prestressed box beam bridges. *PCI Journal*, Vol. 43, No. 2, pp. 72–79.

Liu, Z. 2018. Evaluation of an innovative joint design for the adjacent box beam bridges. PhD dissertation. Iowa State University, Ames, IA.

Liu, Z., A. A. Semendary, and B. M. Phares. 2022. Numerical investigation on early-age performance of ultra-high performance concrete shear keys between an adjacent prestressed concrete box beams. *Advances in Structural Engineering*, Vol. 25, No. 3, pp. 511–521.

Liu, Z., and B. M. Phares. 2022. Field demonstration of an innovative box beam connection. *Journal of Bridge Engineering*, Vol. 28, No. 1.

Liu, Z., and B. M. Phares. 2019. Small-scale investigation on wide longitudinal joints filled with shrinkage-compensated concrete for adjacent box beam bridges. *Journal of Bridge Engineering*, Vol. 24, No. 12.

Liu, Z., and B. M. Phares. 2020. Material selection for the joint between adjacent box beams. *Journal of Materials in Civil Engineering*, Vol. 32, No. 4.

Liu, Z., B. M. Phares, W. Shi, and B. Shafei. 2020. Full-scale evaluation of an innovative joint design between adjacent box beams. *Transportation Research Record*, Vol. 2674, No. 2, pp. 33–44.

Miller, R. A., G. M. Hlavacs, T. Long, and A. Greuel. 1999. Full-scale testing of shear keys for adjacent box girder bridges. *PCI Journal*, Vol. 44, No. 6, pp. 80–90.

Phares, B. M., L. Greimann, Z. Liu, and K. Freeseman. 2017. *Context-Sensitive Designs: Testing of Multi-Performance Level Box Beam Standards*. Institute for Transportation, Ames, IA.

Sharpe, G. P. 2007. Reflective cracking of shear keys in multi-beam bridges. PhD dissertation. Texas A&M University, College Station, TX.

Shi, W., B. Shafei, Z. Liu, and B. M. Phares. 2019. Early-age performance of longitudinal bridge joints made with shrinkage-compensating cement concrete. *Engineering Structures*, Vol. 197.

Shi, W., B. Shafei, Z. Liu, and B. M. Phares. 2020. Longitudinal box-beam bridge joints under monotonic and cyclic loads. *Engineering Structures*, Vol. 220.

Ulku, E., U. Attanayake, and H. M. Aktan. 2010. Rationally designed staged post-tensioning to abate reflective cracking on side-by-side box-beam bridge decks. *Transportation Research Record*, Vol. 2172, No. 1, pp. 87–95.

Yuan, J., B. A. Graybeal, and K. Zmetra. 2018. *Adjacent Box Beam Connections: Performance and Optimization*. FHWA-HRT-17-093. Federal Highway Administration, Washington, DC.

**THE INSTITUTE FOR TRANSPORTATION IS THE FOCAL POINT FOR TRANSPORTATION
AT IOWA STATE UNIVERSITY.**

InTrans centers and programs perform transportation research and provide technology transfer services for government agencies and private companies;

InTrans contributes to Iowa State University and the College of Engineering's educational programs for transportation students and provides K–12 outreach; and

InTrans conducts local, regional, and national transportation services and continuing education programs.

IOWA STATE UNIVERSITY
INSTITUTE FOR TRANSPORTATION

Visit **InTrans.iastate.edu** for color pdfs of this and other research reports.